Assessing and improving cloud-height based parameterisations of global lightning flash rate, and their impact on lightning-produced NOx and tropospheric composition

5 Ashok K. Luhar[1], Ian E. Galbally[1], Matthew T. Woodhouse[1], and Nathan Luke Abraham[2,3]

[1]CSIRO Oceans and Atmosphere, Aspendale, 3195, Australia
[2]National Centre for Atmospheric Science, Department of Chemistry, University of Cambridge, Cambridge, UK
[3]Department of Chemistry, University of Cambridge, Cambridge, UK

10 *Correspondence to*: Ashok K. Luhar (ashok.luhar@csiro.au)

Abstract. Although lightning-generated oxides of nitrogen (LNO$_x$) account for only approximately 10% of the global NO$_x$ source, it has a disproportionately large impact on tropospheric photochemistry due to the conducive conditions in the tropical upper troposphere where lightning is mostly discharged. In most global composition models, lightning flash rates used to calculate LNO$_x$ are expressed in terms of convective cloud-top height via the Price and Rind (1992) (PR92)

15 parameterisations for land and ocean. We conduct a critical assessment of flash-rate parameterisations that are based on cloud-top height and validate them within the ACCESS-UKCA global chemistry-climate model using the LIS/OTD satellite data. While the PR92 parameterisation for land yields satisfactory predictions, the oceanic parameterisation underestimates the observed flash-rate density severely, yielding a global average of 0.33 flashes s^{-1} compared to the observed 9.16 flashes s^{-1} over the ocean and leading to LNO$_x$ being underestimated proportionally. We formulate new/alternative flash-rate

20 parameterisations following Boccippio's (2002) scaling relationships between thunderstorm electrical generator power and storm geometry coupled with available data. While the new parameterisation for land performs very similar to the corresponding PR92 one as would be expected, the new oceanic parameterisation simulates the flash-rate observations more accurately, giving a global average of 8.84 flashes s^{-1}. The use of the improved flash-rate parameterisations in ACCESS-UKCA changes the modelled tropospheric composition—global LNO$_x$ increases from 4.8 to 6.6 Tg N yr^{-1}; the ozone (O$_3$)

25 burden increases by 8.5%; there is an increase in the mid- to upper-tropospheric NO$_x$ by as much as 40 ppt; a 13% increase in the global hydroxyl (OH); a decrease in the methane lifetime by 6.7%; and a decrease in the lower tropospheric carbon monoxide (CO) by 3–7%. Overall, the modelled tropospheric NO$_x$ and ozone are improved compared to observations, particularly in the Southern Hemisphere and over the ocean.

1 Introduction

Oxides of nitrogen ($NO_x \equiv NO$ (nitric oxide) + NO_2 (nitrogen dioxide)) play an important role in tropospheric chemistry by acting as a precursor to ozone (O_3) and the hydroxyl (OH) radical, which are the principal tropospheric oxidants (Labrador et al., 2005). As a greenhouse gas, O_3 is most potent in the upper troposphere, whereas near the Earth's surface it is an air pollutant, adversely impacting human health and plant productivity. The OH radical plays a critical role in the chemical cycles of many trace gases, such as methane (CH_4), in the atmosphere.

Lightning is the dominant source of NO_x in the middle to upper troposphere, and the only direct natural source remote from the Earth's surface (Schumann and Huntrieser, 2007; Banerjee et al., 2014). Lightning predominantly occurs over land in the tropics with deep atmospheric convection. The extreme heat in a lightning flash channel in the atmosphere, which can extend over tens of kilometres, allows for the dissociation of nitrogen (N_2) and oxygen (O_2) molecules. The dissociation products combine to form nitric oxide (NO) which quickly oxidises to form nitrogen dioxide (NO_2), and an equilibrium between NO and NO_2 is reached (Finney et al., 2014). A large uncertainty in the amount of NO_x produced by lightning has been reported, with most global estimates ranging between 2 and 8 Tg nitrogen (N) per year (Schumann and Huntrieser, 2007).

Although lightning accounts for only approximately 10% of the global NO_x source, the lightning-generated NO_x (referred to as LNO_x) has a disproportionately large contribution to the tropospheric burdens of O_3 and OH (Murray, 2016). For example, although LNO_x emissions are of similar magnitude as those from biomass burning or soils, their contribution to the total tropospheric ozone column is about three times larger (Dahlmann et al., 2011). This is because in the middle to upper troposphere where LNO_x is directly released, the O_3 production efficiency per unit NO_x is much higher (~ 100 molecules O_3 per molecule NO_x) than that near the surface (~ 10–30 molecules O_3 per molecule NO_x) as a result of the higher amount of UV radiance, lower concentrations and longer lifetimes of NO_x (a few days rather than hours), and lower temperatures affecting ozone loss chemistry at such altitudes (e.g. Williams, 2005; Dahlmann et al., 2011). Of any major emission source, variability in global mean OH is most sensitive to LNO_x (Murray, 2016). Using a global chemistry transport model, Labrador et al. (2005) observed marked sensitivity of NO_x, O_3, OH, nitric acid (HNO_3) and peroxyacetyl-nitrate (PAN) to the magnitude and vertical distribution of LNO_x. Modelling studies by Grewe et al. (2007) and Dahlmann et al. (2011) found that of all the major sources of NO_x, LNO_x is the dominant source for tropospheric ozone (up to 40%) in the tropics and Southern Hemisphere.

LNO_x is also important when studying natural variability of tropospheric composition because lightning occurrence is influenced by natural climate variability drivers such as El Niño and La Niña in the tropics. Similarly, potential changes in deep convection as a result of future climatic change has a bearing on LNO_x and thus tropospheric ozone and associated radiative feedbacks, and some of these have been explored through modelling (e.g. Banerjee at al., 2014, 2018; Iglesias-Suarez et al., 2018). In addition, lightning intensity and distribution, and its uncertainty, in a future climate has implications for projections of lightning-induced fire activity (Krause et al., 2014).

A realistic representation of LNO$_x$ source strength and its global distribution is thus of vital importance for understanding tropospheric chemistry and its impact. In most global circulation models used for climate applications, convection is diagnosed/parameterised (i.e. clouds are not explicitly resolved) with limited cloud microphysics. A pragmatic way to predict lightning flash rates in these models is to use parameterisations based on simple physics of electrical charge and

5   correlations between the flash rate and appropriate parameters representing convection.

The most common conceptual model used to compute the amount of LNO$_x$ in global models is

$$LNO_x = F \times P_{NO}, \qquad\qquad (1)$$

where F is the lightning flash rate and P_{NO} is the amount of NO produced per flash. This calculation is carried out in atmospheric models by first calculating the lightning flash rate within a model grid column at every model time step, partitioning it into intra-cloud (IC) and cloud-to-cloud (CC) flash-rate components, applying an amount of NO mass

10   produced per flash, and then vertically distributing the calculated NO mass in the column.

Various approaches to estimate lightning flash rate in global models have been followed in the past. Assuming an electric dipole structure for a thunderstorm with two equal but opposite charge volumes, separated by a distance of the order the vertical cloud dimension as developed by Vonnegut (1963) and Williams (1985), Price and Rind (1992, hereafter PR92) developed simple empirical parameterisations for calculating lightning flash rate in terms of convective cloud-top height

15   over land and ocean. Flash-rate parameterisations based on convection parameters other than cloud-top height have also been developed, e.g. convective precipitation and upward mass flux (Allen and Pickering, 2002); convective available potential energy (CAPE) (Choi et al., 2005), cold-cloud depth (Futyan and Del Genio, 2007), maximum vertical velocity and updraft volume (Deierling and Petersen, 2008), upward cloud ice flux (Finney et al., 2014; 2016), product of CAPE and precipitation rate (Romps et al., 2014; Zhu et al., 2019), and multi-parameter regression fits (Luo et al., 2017).

20   The PR92 parameterisations are by far the most widely used ones by default in global chemistry transport models (CTMs) and coupled chemistry-climate models, such as GEOS-Chem (Hudman et al., 2007), MOZART (Emmons et al., 2020), CAM-Chem (Lamarque et al., 2012), ECHAM5/MESSy (Jöckel et al., 2006), and UM-UKCA (Archibald et al., 2020), perhaps primarily because they are based on convective cloud-top height which can be easily diagnosed from a model's convection scheme. Additionally, with its use of an electric dipole structure for a thunderstorm, the framework underlying

25   the PR92 parameterisations has some theoretical support. The PR92 parameterisations also perform reasonably well. For example, Clark et al. (2017) tested flash-rate parameterisations based on cloud-top height, cold cloud depth, mass flux, convective precipitation rate, and cloud-top height with column-integrated cloud droplet number concentration, in a global model, and found that the PR92 parameterisations had the best correlation with the observations, but a higher value of the spatial standard deviation compared to observations due to a large land-ocean contrast in this parameterisation. Finney et al.

30   (2014) found that the PR92 lightning flash parameterisation had considerable biases compared to satellite observations of

spatial flash density but performed 2nd best (behind their parameterisation based on ice flux) out of the 5 parameterisations tested. A recent comparison by Gordillo-Vázquez et al. (2019) of six flash-rate parameterisation schemes showed a relatively good performance by those based on cloud-top height. However, a number of global modelling studies has demonstrated that the PR92 parameterisations underestimate the lightning flash density over the ocean compared to satellite observations

5   (Allen and Pickering, 2002; Tost et al., 2007; Finney et al., 2014, 2016; Clark et al. (2017). The performance of the PR92 flash-rate parameterisations has not yet been tested properly for their land and ocean components separately.

In this paper, we critically assess the performance of currently used flash-rate parameterisations for land and ocean based on convective cloud-top height. We also derive new/alternative flash-rate parameterisations following Boccippio's (2002) (Bo02) scaling relationships founded on theory linking thunderstorm electrical generator power and storm geometry applied

10   to the available data. We implement in a global chemistry-climate model, viz. ACCESS-UKCA (Woodhouse et al., 2015), (a) these new parameterisations, (b) an oceanic flash-rate parameterisation suggested by Michalon et al. (1999) (Mi99), and (c) use the standard PR92 flash-rate parameterisation as a default. The model results are tested using global satellite data of flash density from the Optical Transient Detector (OTD) and Lightning Imaging Sensor (LIS) (Cecil et al., 2014), which are available as global climatological, inter-annual and seasonal distributions. The veracity of the new modelled LNO_x estimates

15   are examined through comparison of modelled and reanalysis tropospheric NO_2 column amounts. The impacts of the modelled LNO_x based on the new flash-rate parameterisations on tropospheric composition involving NO_x, ozone, the hydroxyl radical, methane lifetime, and carbon monoxide are examined, including comparison with observations where available.

2 The ACCESS-UKCA global chemistry-climate model

20   We use the United Kingdom Chemistry and Aerosol (UKCA) global atmospheric composition model (Abraham et al., 2012; http://www.ukca.ac.uk) coupled to ACCESS (Australian Community Climate and Earth System Simulator) (Bi et al., 2013; Woodhouse et al., 2015). In our simulations, ACCESS is essentially the same as the U.K. Met Office Unified Model (UM) (vn8.4) since the ACCESS specific ocean and land-surface components are not invoked as the model is run in atmosphere-only mode with prescribed monthly-mean sea surface temperature (SST) and sea ice fields, and the UM's original land-

25   surface scheme (viz. JULES) is used. The atmosphere component of the UM vn8.4 is the Global Atmosphere (GA 4.0) (Walters et al., 2014). The UKCA configuration used here is the so-called StratTrop (or Chemistry of the Stratosphere and Troposphere (CheST)) (Archibald et al., 2020), which, in essence, combines the tropospheric chemistry scheme described by O'Connor et al. (2014) and the stratospheric chemistry as described by Morgenstern et al. (2009). The tropospheric chemistry scheme includes the O_x, HO_x and NO_x chemical cycles, and the oxidation of CO, methane, and other volatile

30   organic carbon species (e.g. ethane, propane and isoprene). The Fast-JX photolysis scheme (Neu et al. 2007; Telford et al. 2013) is used, and ozone is coupled interactively between chemistry and radiation. The aerosol component includes sulphur chemistry. The total number of reactions, including aerosol chemistry, is 306 across 86 species.

The atmospheric model has a horizontal resolution of 1.875° in longitude and 1.25° in latitude, and 85 staggered terrain-following hybrid-height levels extending from the surface to 85 km (the so-called N96L85 configuration). The vertical resolution decreases with height, with the lowest 65 levels (up to ~ 30 km) lying within the troposphere and lower stratosphere. The UKCA timestep is 60 min and the model physics timestep is 20 min. A global monthly-varying emissions database for reactive gases and aerosols is used, which includes both anthropogenic, biomass burning and natural components, whereas for carbon dioxide, methane, nitrous oxide and ozone depleting substances, concentrations are prescribed instead of emissions (Woodhouse et al., 2015).

The ACCESS-UKCA setup used here incorporates some additional modifications compared to the base UM-UKCA version 8.4, and these include:

- Dry deposition of ozone to the ocean is now based on a process-based scheme developed by Luhar et al. (2018) (the Ranking 1 configuration in their Table 1).

- Dry deposition of all relevant species is applied at the lowest model level, instead of it being distributed through the vertical extent of the atmospheric boundary layer (Luhar et al., 2017).

- The coefficient 8.53 is corrected to 4.8 in the following branching ratio expression used to compute the rate constant k_2 (cm^3 $molecule^{-1}$ s^{-1}) for the chemical reaction $HO_2 + NO \rightarrow HNO_3$:

$$k_2/k = \{[(530 \pm 10)/T] + 4.8 \times 10^{-4} \times P - (1.73 \pm 0.07)\}/100, \quad (2)$$

where pressure P is in hPa and temperature, T is in K, and k is the rate constant (cm^3 $molecule^{-1}$ s^{-1}) for the chemical reaction $HO_2 + NO \rightarrow NO_2 + HO$. The coefficient 8.53 is correct when P is expressed in Torr (Butkovskaya et al., 2007), but it should be 4.8 when P is in mbar[1].

- In the parameterisation $k = c_0 \times 10^{-12} \exp(270/T)$, the model uses $c_0 = 3.3$ for this reaction, but in the branching ratio Eq. (2) it uses $c_0 = 3.6$, which we change to 3.3 for consistency.

The above changes lead to an increase in the tropospheric ozone burden (the first two changes together by ~ 7% and the last two together by ~ 5%).

Another change is that we have backported the LNO_x subroutines from a more recent version of the model (at UM vn11.0) to vn8.4. This is to ensure that any refinements that may have occurred in the new version are used in our study. However, it is found that there are no major LNO_x parameterisation differences between the two versions, with the new version continuing to use the original PR92 flash-rate parameterisations.

---

[1] This inconsistency stems from a typo in the document "IUPAC Task Group on Atmospheric Chemical Kinetic Data Evaluation – Data Sheet I.A3.45 NOx15" (http://iupac.pole-ether.fr/htdocs/datasheets/pdf/NOx15_HO2_NO.pdf) in which a constant of 8.53 instead of 4.8 is mistakenly specified in the branching ratio expression in the "Rate coefficient data" table.

2.1 Implementation of lightning flash-rate parameterisation in the model

In ACCESS-UKCA, convective cloud bottom level (H_b) and top level (H) are diagnosed from the UM convection scheme. This scheme represents the sub-grid scale transport of heat, moisture and momentum associated with cumulus clouds within a grid box. The scheme uses a mass flux convection scheme based on Gregory and Rowntree (1990) with various extensions

5 to include downdraughts and convective momentum transport (Walters et al., 2014). The scheme consists of three stages: (a) diagnosis to determine whether convection is possible from the boundary layer, (b) a call to the shallow or deep convection scheme for all points diagnosed deep or shallow by the first step, and (c) a call to the mid-level convection scheme for all grid points. Examples of evaluation of the distribution of cloud depths simulated by the UM include those by Klein et al. (2013) and Hardiman et al. (2015).

10 A minimum convective cloud thickness ($H - H_B$) of 5 km is required for the lightning NO$_x$ to be activated (the use of 5 km is based on the range of data used to develop the flash-rate formulas by PR92), and the model diagnosed H is used in the flash-rate parameterisations, which calculate the lightning flash rate (F, flashes per minute) as a function of and H (km) (see Section 3.2).

The PR92 flash-rate expressions (discusses later in Section 3.2) were developed based on observations of individual

15 thunderstorms. Price and Rind (1994) developed a spatial calibration factor (c) to adjust these expressions for varying model resolutions:

$$c = 0.97241 \exp(0.048203 \, \Delta x \, \Delta y), \tag{3}$$

where Δx is the longitudinal resolution and Δy is the latitudinal resolution of the model (in degrees).

The total flash rate (f) within a grid cell (flashes per minute per grid box) is then calculated as

$$f_{L,O} = \frac{c \, F_{L,O} \, A}{A_c}, \tag{4}$$

where A is the model grid box area (which is a function of latitude), A_c is the area of model grid box centred at 30°N (Allen

20 and Pickering, 2002), and the subscripts L and O to refer to land/continental and ocean/marine, respectively.

The total flash rate $f_{L,O}$ is then divided into proportion of flashes that are cloud-to-ground (CG) and those that are intracloud (IC) using the method suggested by Price and Rind (1993) based on the thickness of the cold cloud region (0°C to cloud top) in thunderstorms which in turn is parameterised in terms of latitude. CG flashes are about 20–25% of the total (Barthe and Barth, 2008; Price and Rind, 1994), which we find is also the case with our model.

25 ### 2.2 Production of NO per flash

Both the moles of NO produced per flash, P_{NO}, and the variation of this parameter between CG and IC flashes are poorly constrained by atmospheric observations. The overall rate, P_{NO}, regulates the amount of nitrogen oxides produced by

lightning, whereas the variation of P_{NO} between CG and IC flashes regulates the level at which lightning nitrogen oxides are introduced into the atmosphere, both are critical variables. In this study, P_{NO} is set at the model default value 330 moles NO per flash irrespective of whether a flash is IC or CG. This value is comparable to 310 moles NO per flash obtained by Miyazaki et al. (2014) using an assimilation of multiple satellite measurements of NO_2, O_3, HNO_3 and CO, and the LIS/OTD

5   flash data into a global CTM for the year 2007.

In bottom-up models, in addition to flash rate, P_{NO} is a key source of uncertainty, with a review by Schumann and Huntrieser (2007) suggesting a range of ~ 33–660 and an average of 250 moles NO per flash. This large range, in part, reflects spatial variation in the frequency and uncertainty in the relative yield of CG and IC flashes, which may involve a varying level of dependencies on environmental variables such as peak current, rate of energy dissipation, channel length, air density, and

10   strokes per flash (Murray et al., 2016). For example, some modelling studies consider that the less frequent CG flashes yield a greater amount of NO per flash than IC flashes (Price et al., 1997; Luo et al., 2017), whereas in others both CG and IC flashes yield the same amount of NO on average (DeCaria et al., 2005; Ott et al., 2007). A few studies suggest that P_{NO} may not be constant over the globe, with higher production rates in extratropics than tropics (Murray et al., 2012) and globally variable production rates (Miyazaki et al., 2014). Details about P_{NO} and global LNO_x reported in previous studies are given

15   in Section 3.7.1.

3 Flash-rate parameterisations based on convective cloud-top height and LNO_x

The approach of parameterising lightning flash frequency in terms of cloud-top height has its origins in the simple scaling relationships suggested by Vonnegut (1963) for the electrical power output of a thundercloud with the cloud size. Vonnegut's model assumes an electric dipole structure with two equal but opposite charge volumes, separated by a distance

20   on the order of the vertical cloud dimension, and a cloud aspect ratio of approximately unity. The charge transport velocity (charging current) that supports the dipole, flows in the vertical and is assumed to exist across the horizontal cross-section of the cloud. The electrical power generated is proportional to the fifth power of cloud dimension and the lightning flash rate is proportional to the electrical power generated. Williams (1985) extended this work using Vonnegut's (1963) model and available atmospheric observations over land to demonstrate from observations that (a) the convective velocity for clouds

25   ranging in size from a few kilometres to 17 km is proportional to the size of the cloud and (b) cloud height and flash-rate data from three US locations (New England, Florida and New Mexico) are in good agreement with the predicted slope of 5 from Vonnegut (1963). An important consequence of the last finding is that charge transport velocity must scale with cloud dimension, in the same way as convective velocity does. However, as Williams (1985) writes, this does not establish whether convective motion or falling precipitation is directly responsible for the charge separation.

3.1 Boccippio's (2002) extension of Vonnegut's model and derivation of scaling relationships for land and ocean

Boccippio (2002) presents a systematic physical account of Vonnegut's (1963) model and the subsequent work on this issue by Williams (1985), PR92 and others. Boccippio (2002), using the laws of electricity, derived a fundamental scaling relationship between thunderstorm electrical generator power and storm geometry, which provides a possible theoretical basis for linking lightning to thunderstorm dynamics, microphysics, and geometry. Boccippio (2002) takes Vonnegut's conceptualized thunderstorm of a quasi-steady state electrical dipole, with the horizontal and vertical scales of the two dipole charge centres comparable and varying with storm scale. The storm generator current is conceptualized as a net charge transport velocity, which maintains the dipoles. The electrical generator power (watts) is calculated as the generator current multiplied by the potential drop between the dipoles. The generator power is further expressed by assuming tangential spherical charge centres with volumetric charge density ($\pm\rho$) and radius R, maintained by a generator current density (= charge density × charge transport velocity). Scale similarity between horizontal and vertical dimensions is invoked, and the dipole separation and size of the spherical charge centres are assumed to vary linearly with cloud-top height, a more readily observable parameter. The lightning flash rate is taken to vary linearly with lightning power dissipation, the latter is assumed to vary monotonically with generator power. A further significant and explicit simplification replaces charge transport velocity with storm updraft velocity w. With the assumptions above, the flash rate F scaling relation is

$$F \sim \gamma\,\varepsilon^{-1}\rho^2 w\,H^4, \tag{5}$$

where H is cloud-top height (m), w is updraft velocity (m s^{-1}), ρ is charge density (coulomb m^{-3}), ε is permittivity constant (coulomb^2 joule^{-1} m^{-1}), and the coefficient γ has units of joule^{-1}. The variability in the charge density of the dominant dipole regions is taken to be small, and thus can be treated as a prescribed constant.

In all the following parameterisations, $F_{L,O}$ is in flashes per minute, H is in km, and w is in m s^{-1}.

It is apparent that in the above approach, flash rate is set by storm dimension, with a small direct contribution from generator current density (which is taken to vary linearly with updraft velocity). In the case where $w(z)$ for land and ocean are considered to be power law fits of H, i.e.

$$w_{L,O} = k_{L,O}\,H^{a_{L,O}}, \tag{6}$$

the above approach based on Eq. (5) leads to the following self-consistent scaling relationships, where the coefficient k_1 ($\sim \gamma\,\varepsilon^{-1}\rho^2$) is (supposed to be) invariant, and $a_{L,O}$ and $k_{L,O}$ are other coefficients for land and ocean (Boccippio, 2002):

$$F_{L,O} = k_1\,k_{L,O}\,H^{a_{L,O}+4}, \tag{7}$$

$$F_{L,O} = k_1\,k_{L,O}^{-4/a_{L,O}}\,w^{1+(4/a_{L,O})}. \tag{8}$$

These self-consistent scaling relationships are central to this study.

Using these scaling relationships, the data of Williams (1985), PR92 and LIS satellite data, Boccippio (2002) derived

$$F_L = 2.13 \times 10^{-5} H^{5.09} \tag{9}$$

(note there is a negative sign missing in the first exponent of this equation in Boccippio (2002)), and

$$F_O = 4.09 \times 10^{-5} H^{4.38}, \tag{10}$$

where $k_1 = 1.4314 \times 10^{-5}$ was used in deriving the relationships (9) and (10), which are plotted in Figure 1.

3.2 Price and Rind's (1992) (PR92) parameterisations

5   PR92, following Vonnegut (1963) and Williams (1985), present a simple lightning parameterisation for calculating global lightning distributions. Using continental storm observations used by Williams (1985) to establish the fifth power dependency, PR92 derived an empirical relationship between continental lightning flash rate and H

$$F_L = 3.44 \times 10^{-5} H^{4.9}. \tag{11}$$

There were no direct F vs. H data to fit a relationship similar to Eq. (11) for the marine environment. Therefore, PR92 made the assumption that the charge separation velocity and the convective updraft velocity are equal, noted that an increase in the

10   intensity of convective updrafts enhances cloud electrification, and derived empirical relations based on observations between maximum updraft velocity (w, m s^{-1}) and H (km) for continental and marine clouds

$$w_L = 1.49 H^{1.09}, \tag{12}$$

$$w_O = 2.86 H^{0.38}. \tag{13}$$

Eliminating H from Eqs. (11) and (12) yields

$$w_L = 14.66 F_L^{0.22}. \tag{14}$$

Now, PR92 made the crucial assumption that Eq. (14) is independent of location, so is valid for the marine environment too. Thus, by substituting Eq. (8) into Eq. (13) they obtained the following expression for marine environment

$$F_O = 6.4 \times 10^{-4} H^{1.73}. \tag{15}$$

15   (Our calculation suggests that the coefficient 6.4 in the above equation should actually be 5.94.) The relationships (11) and (15) are plotted in Figure 1, which show that the oceanic flash frequencies that are roughly 2 to 3 orders of magnitude smaller than those obtained for continental clouds.

According to Boccippio (2002), the derivation of Eq. (15) includes significant formal inconsistency and yields non-physical cloud-height predictions upon inversion and other non-physical behaviours, e.g. inverse relationship between updrafts and

20   cloud heights.

The PR92 parameterisations (11) and (15) are widely used in global chemistry transport models and coupled chemistry-climate models.
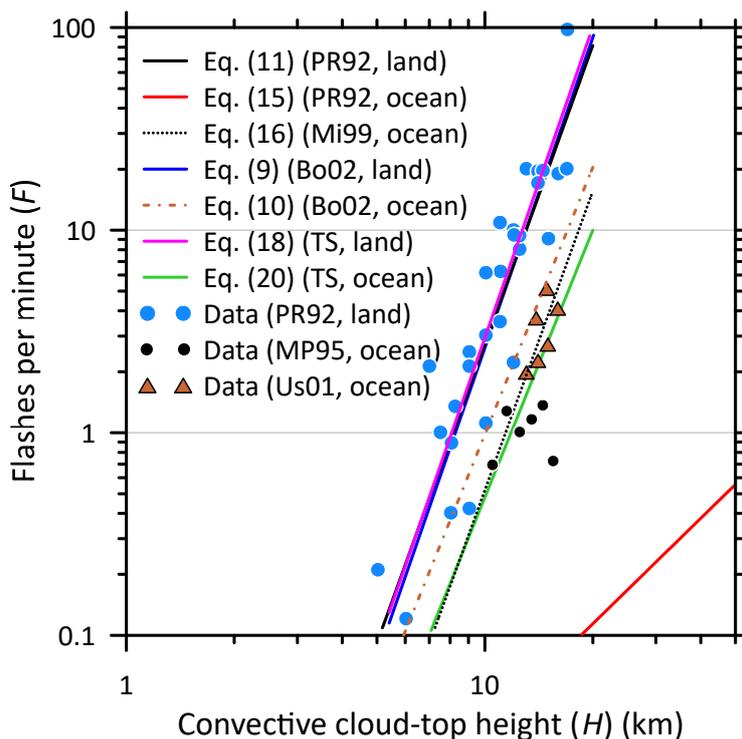
Figure 1: Various relationships, including those from this study (TS), between lightning frequency F (flashes per minute) and convective cloud-top height H (km). The land data points are from PR92, and the ocean data are from Molinié and Pontikis (1995) (MP95) and Ushio et al. (2001) (Us01); Bo02 – Boccippio (2002), Mi99 – Michalon et al. (1999), and PR92 – Price and Rind (1992).

3.3 Michalon et al.'s (1999) ocean parameterisation

Michalon et al. (1999) identified that the PR92 parameterisation, when used in global models, was producing lightning flash frequencies that did not agree with observations. To address this, they proposed that cloud electrification is directly related to cloud droplet concentration (N) and droplet size, and derived $F = A N^{2/3} H^5$, where A is a proportionality constant. They retained the continental PR92 expression (11) by considering that it has been directly calibrated by using observed F and H

10

values, and used it for the ocean by multiplying it with a factor of $(N_O/N_L)^{2/3}$ assuming that cloud droplet concentrations for continental (N_L) and marine (N_O) clouds are different:

$$F_O = 3.44 \times 10^{-5} \left(\frac{N_O}{N_L}\right)^{2/3} H^{4.9} = 6.57 \times 10^{-6} H^{4.9}, \tag{16}$$

where two "standard" continental and maritime cloud droplet concentrations of $N_L = 600$ and $N_O = 50$ per mg of air, respectively, were used. Eq. (16) is plotted in Figure 1. One factor for a smaller droplet concentration in marine clouds is

5   suggested to be more intense droplet coalescence in such clouds (Rosenfeld and Lensky, 1998).

In the above approach, the values of N_L and N_O are not well constrained. There is a large variability in cloud droplet concentration over land and ocean, as reflected in values observed in field experiments as well as those prescribed in cloud microphysics schemes in global models (convective cloud droplet concentrations are not usually predicted in global climate models) (Rosenfeld and Lensky, 1998; Gultepe and Isaac, 2004). Boccippio (2002) cautions against this approach, and we

10   suggest that given the uncertainty in the mean droplet concentrations, the approach of Michalon et al. (1999) is essentially empirical.

3.4 This study: Alternative flash-rate parameterisations

The following includes (a) the reanalysis of the Williams (1985) and PR92 data for lightning flashes versus cloud top height over land into the self-consistent scaling relationships framework of Boccippio (2002) and (b) the derivation of a new

15   relationship for the oceanic environment using these scaling relationships.

For land, considering initially the relationship of updraft velocity with cloud-top height: equating the scaling relationship Eq. (6) with the observed maximum updraft velocity from PR92 given in Eq. (12) gives $k_L = 1.49$ and $a_L = 1.09$. Substituting these values into the relationship of flash rate with cloud-top height Eq. (7) yields

$$F_L = 1.49 \, k_1 H^{5.09}. \tag{17}$$

At this stage k_1 is undetermined. We proceed by fitting Eq. (17) directly to the F vs. H data for land reported by Williams

20   (1985) and compiled by PR92 (which are reproduced in Figure 1 as blue solid circles). This gives $k_1 = 1.612 \times 10^{-5}$ and

$$F_L = 2.40 \times 10^{-5} H^{5.09}. \tag{18}$$

The relationships PR92 Eq. (11), Boccippio (2002) Eq. (9) and this study (TS) Eq. (18) are presented in Figure 1 along with the F vs. H data just discussed. Although these behaviours look almost identical and are well within the scatter of the data, Eq. (18) shows a slightly higher flash rate for higher H than the other two. The almost fifth power dependence on H makes F_L very susceptible to even small changes in the F_L-H relationship and in how cloud-top height is calculated in the model.

Note that variation of flash rate at higher H is important for both global distributions of flash rate and how it may change with changing convective activity, e.g. climate change.

Concerning the oceanic parameterisation: there are limited data on flash rate versus cloud-top height for marine environments. Figure 1 presents Ushio et al.'s (2001) (Us01) data over the ocean in the tropics and extratropics (their Figure 3b and 3d), which they obtained by averaging flash rates every 1 km in cloud height. These are shown as triangles in Figure 1. Also shown are the Molinié and Pontikis' (1995) (MP95) flash-rate data over French Guyana coastal zone which we averaged over every 1 km in cloud height for heights greater than 10 km (below this height, the number of data points is not sufficient for averaging). Because these are coastal observations, it is possible that the air masses in which the thunderstorm clouds developed could be mixed air masses (i.e. both continental and marine). However, these data do show a qualitative agreement with the Ushio et al. (2001) data in Figure 1.

Applying the scaling relationships (Boccippio 2002) to obtain an equivalent relationship for marine clouds involves equating Eq. (6) with the observed oceanic convective updraft velocity versus cloud top height from PR92 given in Eq. (13). This yields $k_O = 2.86$ and $a_O = 0.38$. Substituting these into the scaling relationship Eq. (7) gives

$$F_O = k_1 \times 2.86 \times H^{4.38} = A_O H^{4.38}. \tag{19}$$

For this study, fitting Eq. (19) to the ocean data leads to $A_O = 2 \times 10^{-5}$ (which gives $k_1 = 0.7 \times 10^{-5}$) and

$$F_O = 2.0 \times 10^{-5} H^{4.38}. \tag{20}$$

This marine parameterisation yields flash rates that are approximately an order of magnitude smaller than the PR92 continental formula and roughly two orders of magnitude larger than the PR92 marine parameterisation. In Figure 1 are shown the relationships for lightning flash rates and associated cloud-top height over the ocean for PR92, Boccippio's (2002) Eq. (10), Michalon et al. (1999) and this study (TS) Eq. (20). Clearly the PR92 ocean equation is unrealistic, and the relationship of Boccippio (2002) gives marine flash rates that are twice as large as Eq. (20) and are not supported by the data plotted. The relationships of Michalon et al (1999) and this study group together around the oceanic data.

The values of k_1 implicit in Eqs. (18) and (20) are different for land and ocean, although as per Boccippio's (2002) theory, they should be the same (as used in deriving Eqs. (9) and (10)). This difference may suggest possible differences in cloud microphysics between land and ocean, which Boccippio's (2002) generator power framework does not include. If we use the same logic as by Michalon et al. (1999) in deriving Eq. (16), then the different values of k_1 in Eqs. (18) and (20) for land and ocean can be interpreted in terms of the values of N_O and N_L being different.

3.5 Global model runs with various flash-rate parameterisations

In order to assess the above flash-rate parameterisations against global lightning flash observations, and to investigate how they influence tropospheric composition via their impact on LNO_x generation, we conduct the following four runs of the ACCESS-UKCA global chemistry-climate model incorporating the five specified flash-rate parameterisations:

5
- Run 1 (PR92): The default PR92 parameterisations: continental Eq. (11) and marine Eq. (15),
- Run 2 (this study - TS1): The new parameterisations: continental Eq. (18) and marine Eq. (20),
- Run 3 (this study - TS2): The PR92 continental Eq. (11) and new marine Eq. (20), and
- Run 4 (Mi99): The PR92 continental Eq. (11) and Michalon et al.'s (1999) marine Eq. (16).

ACCESS-UKCA was setup as a free running simulation for 2 years (2005–2006), and the simulation was started using
10 model initial conditions taken from a previously spun-up, nudged model run. The first year was used as a spin-up period and the model output for the year 2006 used for analysis.

3.6 Comparison of the modelled lightning flash rates with satellite observations

We analyse the global gridded lightning flash data from the Optical Transient Detector (OTD) on the OrbView-1 (formerly MicroLab-1) satellite and the Lightning Imaging Sensor (LIS) on the Tropical Rainfall Measuring Mission (TRMM)
15 satellite, which are described by Cecil et al. (2014) and available from https://lightning.nsstc.nasa.gov/data/data_lis-otd-climatology.html (V2.3.2015). The high resolution ($0.5° \times 0.5°$) mean annual flash climatology (HRFC), low resolution ($2.5° \times 2.5°$) mean annual flash climatology (LRFC), and low resolution ($2.5° \times 2.5°$) monthly time series (LRMTS) data products are useful for our analysis. The climatology and time series data are flash density values with the units of flashes km^{-2} yr^{-1} and flashes km^{-2} day^{-1}, respectively. The OTD data available from July 1995 to January 2000 cover all
20 latitudes, whereas the LIS data available from February 2000 to February 2014 cover $\pm$ 42.5°. The climatology data cover all latitudes. For comparison with the modelled flash parameters, the satellite data were spatially regridded to the model N96 resolution (1.875° longitude $\times$ 1.25° latitude) using the Climate Data Operators (CDO) software.

Table 1 gives the observed and modelled lightning flash frequencies (flashes s^{-1}) averaged over the globe, Northern Hemisphere (NH), Southern Hemisphere (SH), land, and ocean for the four model runs, and these are plotted in Figure 2. In
25 Figure 2a, the observations are the combined LIS and OTD climatological data, whereas in Figure 2b, the observations are the LIS data for the year 2006 which are only available for the latitudinal range $\pm$ 42.5° with the modelled values also given for this range. The observations for the year 2006 are very well correlated to the climatology, and the two are very similar in magnitude as well since most lightning activity would fall within $\pm$ 42.5°. The data show that ~ 80% of the global lightning flashes are over land, and ~ 55% are in the Northern Hemisphere. On average, the default PR92 parameterisations (Run 1)
30 underestimate the flash frequency data by 28% for the globe, by ~ 13% for land, and by ~ 96% for the ocean. Clearly, the oceanic PR92 flash-rate parameterisation Eq. (15) does not work well at all over the ocean, yielding an almost zero flash

frequency compared to the data. In contrast, the new flash-rate parameterisations (Run 2, Eqs. (18) and (20)) greatly improve the estimation of flash frequency over the ocean, with some overestimation (by ~ 15%) of the climatology and giving nearly the same value as the year 2006 observational data. There is an improvement over land too compared to the PR92 formula. Globally, the new parameterisations yield almost the same flash frequency as the data. Both the PR92 and the new

5   parameterisations lead to an almost equal partitioning of flashes in the Northern and Southern hemispheres, compared to ~ 55% in the Northern Hemisphere indicated by the data. As expected, the Run 3 flash rate is nearly the same as that for Run 1 for land, and that for Run 2 for the ocean. For Run 4, with the PR92 continental Eq. (11) and Michalon et al.'s (1999) marine Eq. (16), the flash rate over land is almost the same as Run 1, whereas for the ocean Run 4 gives a flash rate that is about 50% higher than the climatology and 23% higher than the data for 2006.

10
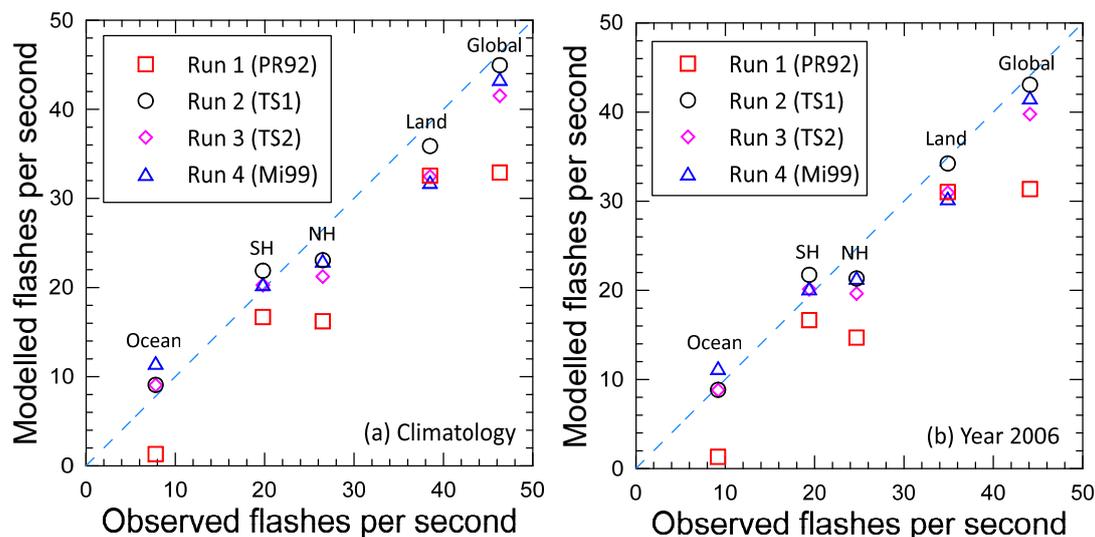
Figure 2: Observed versus modelled flash rates from the four model runs (corresponding to PR92, this study 1 and 2, and Mi99) conducted for the year 2006. The vertical clusters of points are the values over the globe, ocean, land, Southern Hemisphere (SH), Northern Hemisphere (NH). (a) The observations are the LIS/OTD climatological data, and (b) the observations are the LIS data

15   for the year 2006 that are available for the latitude range ± 42.5° (with the modelled values also corresponding to this range).

Table 1: Observed and simulated lightning flash frequencies for the various model runs. The values in the parentheses are for the latitudinal range ± 42.5° (which correspond the latitudinal coverage of the LIS data).

Data/model	Lightning flash frequency (flashes s^{-1})				
	Global	NH	SH	Land	Ocean
LIS/OTD climatology	46.26 (43.55)	26.48 (23.86)	19.78 (19.69)	38.54 (36.00)	7.72 (7.55)
LIS observations – year 2006	(44.08)	(24.73)	(19.35)	(34.92)	(9.16)
Run 1 (PR92)	32.92 (31.36)	16.22 (14.70)	16.70 (16.66)	32.56 (31.03)	0.36 (0.33)
Run 2 (TS1)	44.96 (43.07)	23.07 (21.33)	21.89 (21.74)	35.88 (34.23)	9.08 (8.84)
Run 3 (TS2)	41.53 (39.77)	21.24 (19.64)	20.29 (20.13)	32.47 (30.96)	9.06 (8.81)
Run 4 (Mi99)	43.42 (41.65)	23.03 (21.42)	20.39 (20.23)	31.85 (30.34)	11.57 (11.31)

5 The monthly variation of the observed and modelled flash rates is shown in Figure 3. The observed variation for the year 2006 is very similar to the climatological variation, mostly within the one standard deviation climatological variability shown. The model runs underpredict in spring in both hemispheres and overpredict in autumn in the Southern Hemisphere. In the Northern Hemisphere (Figure 3a), the model simulates the observed variation qualitatively with a peak in July, but while Run 1 underestimates the observed flash rate for all months, the other Runs mostly underestimate during February –
10 May and do well for the other months. In the Southern Hemisphere (Figure 3b), again the model is able to simulate the observed variation well qualitatively, but a significant overprediction for January – April and an underprediction for August – October is apparent. In the global plot (Figure 3c), while Run 1 always underestimates, which is mostly because of its underprediction of the flash rate over the ocean (Figure 3e), the other Runs underestimate in the first three months of the year and overestimates during September – November, and these differences can be explained in terms of the hemispheric
15 differences shown above. The nature of monthly variation in Figure 3d for land-based flash rates is very similar to Figure 3c, indicating that continental flashes dominate the global total. The large underprediction by the PR92 scheme in Run 1 and an overprediction in Run 4 over the ocean can be seen in Figure 3e; there are also differences in the monthly variation.
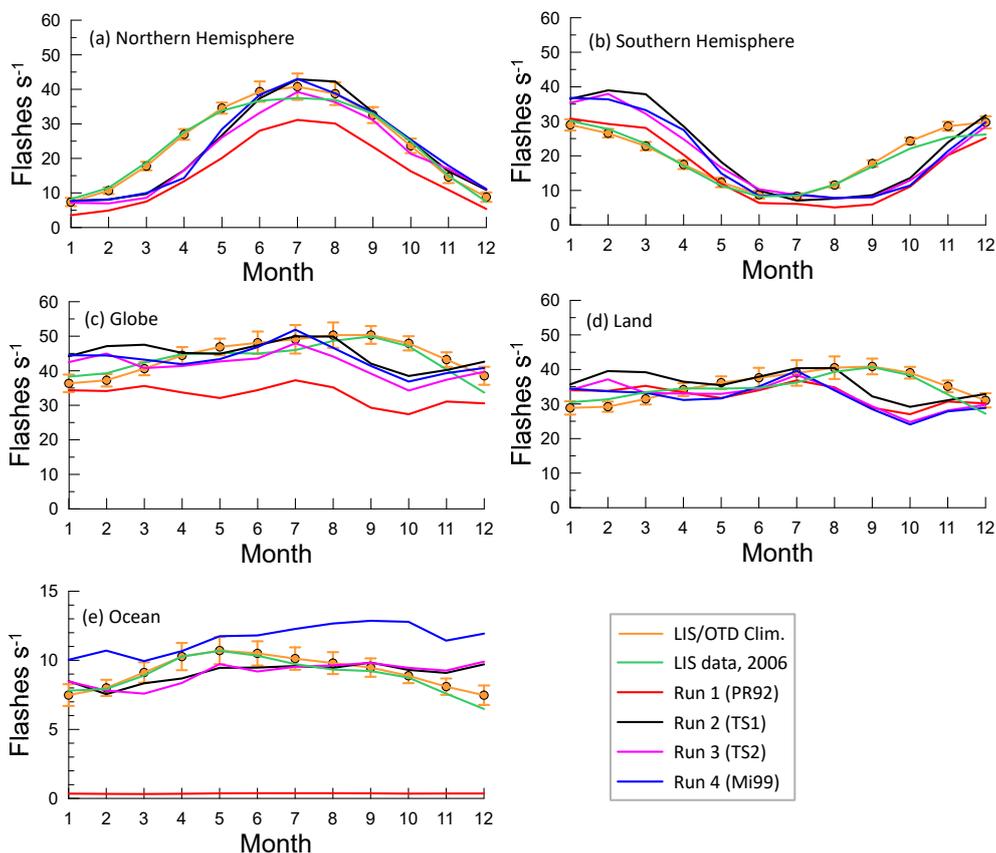
15

Figure 3: Monthly variation of the observed and modelled flash rates from the four model runs for the year 2006: (a) Northern Hemisphere (NH), (b) Southern Hemisphere (SH), (b) ocean, (c) land, (d) globe Southern Hemisphere (SH), and (e) The observations are the LIS/OTD climatological data (with 1 standard deviation variability) and the LIS data for the year 2006.

The normalised mean square error NMSE $= \overline{(M-O)^2}/(\bar{M}.\bar{O})$ calculated for the monthly-varying observed climatology (O) and modelled (M) flash rates shown in Figure 3 are given in Table 2 for the globe, land and ocean. Also given are the values of fractional bias FB $= 2(\bar{O}-\bar{M})/(\bar{O}+\bar{M})$, which varies between -2 (overestimation) and +2 (underestimation). These values confirm, as shown in Figure 2, that the Run 2 flash-rate parameterisations from this study yield the best comparison with the data.

Atmospheric
Chemistry
and Physics
Discussions

Table 2: Normalised mean square error (NMSE) and fractional bias (FB) for the monthly-varying observed climatology and modelled flash rates shown in Figure 3.

Flash-rate scheme	NMSE			FB		
	Globe	Land	Ocean	Globe	Land	Ocean
Run 1 (PR92)	0.164	0.079	18.939	0.343	0.185	1.813
Run 2 (TS1)	0.029	0.048	0.064	0.034	0.088	-0.213
Run 3 (TS2)	0.046	0.084	0.068	0.114	0.188	-0.211
Run 4 (Mi99)	0.031	0.088	0.233	0.069	0.207	-0.449

5

Figure 4 presents the observed and modelled zonal mean flash density (flashes km^{-2} yr^{-1}) over the globe, land, and ocean. All modelled global distributions and the data agree that the flash density is largely concentrated in the tropics. The observed peak for the year 2006 in Figure 4a is better simulated by Runs 2–4 than Run 1. The results over land (Figure 4b) are very similar for all Runs. Over the ocean (Figure 4c), while the default oceanic parameterisation (Run 1) yields a near-zero flash

10 density distribution, the new flash parameterisation (in Runs 2 and 3) performs much better. There are significant distributional differences compared to the data. It is clear in these plots that the observed latitudinal distributions of flash density are wider than the modelled ones, with larger observed flash densities in the subtropics stretching into the mid latitudes (roughly 20–40° in both hemispheres) than modelled. The reason for this may be the inherent limitation of the simple flash parameterisation approach based on convective cloud-top height or uncertainty/biases in the modelled

15 convection (e.g. Allen and Pickering, 2002; Tost et al., 2007). Another potential factor could be greater vertical wind shear outside the tropics which extends the horizontal lightning channel length (Huntrieser et al., 2008), which is not accounted for in the cloud-top height-based approaches.
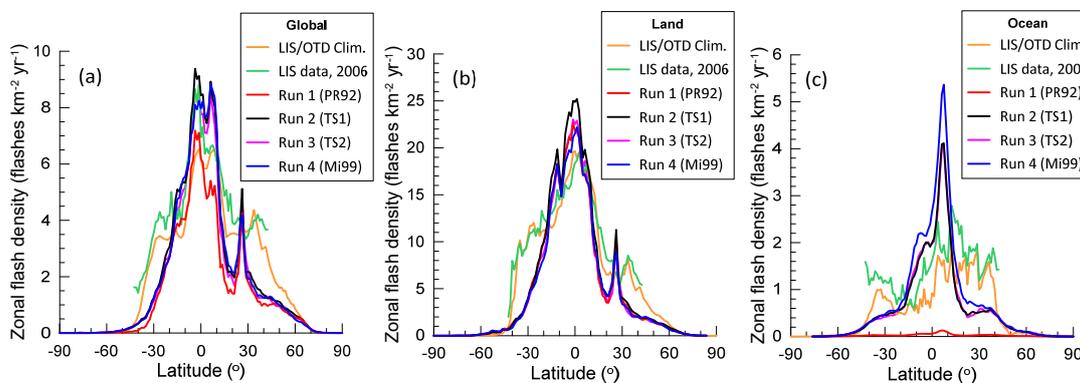
Figure 4: Observed and modelled zonal mean flash densities (flashes km^{-2} yr^{-1}) from the four model runs over the (a) globe, (b) land and (c) ocean. The observations are the LIS/OTD climatology and the LIS data for the year 2006.

Hereafter, we only present plots from Run 1 (default) and Run 2 (new), but the results from Runs 3 and 4 are included in all comparison Tables except Table 5.

Figure 5 compares the various global distributions of the mean annual lightning flash density at N96 resolution. The LIS data for the year 2006 in Figure 5b are only available for the latitudinal range ± 42.5° and have no sampling for some regions within this range. Where there are data, there is a good agreement between the observed distribution in Figure 5b and the LIS/OTD climatology in Figure 5b, showing high flash density over land in the tropics and subtropics, and also lower mid latitudes. There is also some significant flash density over the ocean at these latitudes, particularly over the Pacific, western Atlantic, western Indian Ocean near southern Africa, and the seas around the maritime continent (i.e., largely Indonesia, the Philippines and Papua New Guinea). The distribution modelled using ACCESS-UKCA with the default PR92 flash-rate scheme (Run 1) shown in Figure 5c is very similar to other global modelling studies that use the same PR92 scheme, e.g. Allen and Pickering (2002) using GEOS-STRAT DAS, Tost et al. (2007) using ECHAM5/MESSy, Murray et al. (2012) using GEOS-Chem, Finney et al. (2014) using ERA-Interim reanalyses, Finney et al. (2016) using UM-UKCA vn8.4, and Clark et al. (2017) using CAM5. It is remarkable that the simple PR92 scheme based on the convective cloud-top height is able to simulate the broad observed global distribution of flash density over land, but over the ocean, in contrast to the observations, the scheme predicts almost zero flash density. However, as shown in Figure 5d, ACCESS-UKCA with the new flash-rate parameterisations (Run 2) simulates the oceanic distribution of flash density much better than the PR92 scheme, although it is clear that there are some significant spatial differences (e.g. western Indian Ocean near southern Africa, equatorial Indian Ocean and the Pacific) compared to the corresponding observations and climatology. The modelled flash-density distributions over land in Figure 5c and Figure 5d are nearly the same.
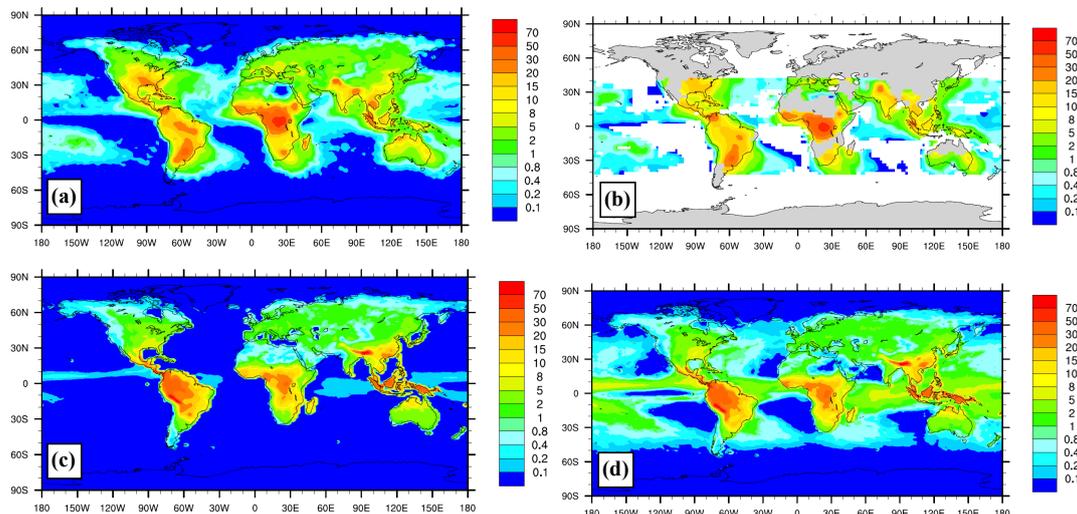
Figure 5: Global distribution of the mean annual lightning flash density (flashes km⁻² yr⁻¹): (a) LIS/OTD satellite climatology, (b)
5 **LIS satellite data for the year 2006 (available only for ± 42.5° latitudes), (c) model simulation with the default PR92 flash-rate**
parameterisations (Run 1), and (d) model simulation with the new flash-rate parameterisations from this study (Run 2).

The area-weighted NMSE, FB and correlation coefficient (r) comparing the spatial patterns of the observed climatology
presented in Figure 5a with the annually-averaged modelled patterns of flash rate are given in Table 3 for the four model

10 runs. The NMSE and FB values clearly show that Run 1 performs the worst, a result dominated by the oceanic component.
While the NMSE values are nearly the same for Runs 2–4, Run 2 has the best FB values. The spatial pattern correlation stays
essentially the same for all Runs (presumably because the underlying independent model variable, the cloud-top height, is
the same in all model runs), and it is lower for the ocean – suggesting that further understanding of convection and lightning
processes and their parameterisations are needed. The global correlations in Table 3 are very similar to those reported by

15 Gordillo-Vazquez et al. (2019) for cloud-height based schemes, but those for the ocean are lower in our study.

Based on the above flash-rate comparisons, Run 2 (TS1) performs the best, followed by Run 3 (TS2), Run 4 (Mi99) and Run
1 (PR92).

Modelled flash rates depend critically on modelled convection parameters (e.g. the cloud-top height) used by flash-rate
parameterisations and on the representativeness of these parameterisations themselves. Thus, it is common in a global model

20 to match the globally averaged modelled lightning flash rate to the observed value, e.g. that based on the LIS/OTD

19

climatology (~ 46 flashes s^{-1}), by applying a constant scaling factor to the modelled global flash-rate spatial distribution (e.g. Gordillo-Vázquez et al., 2019) after doing a model pre-run. However, such a scaling would be misleading when there are large differences in the spatial representativeness of the flash rate computed by the parameterisation used in a model. For example, scaling the PR92 derived global flash-rate distribution would over-adjust the flash rate over land to compensate for

5 the deficiency in the oceanic parameterisation. (Scaling is also applied to tune moles NO produced per flash to get a desired total global LNO$_x$ amount, as per Eq. (1).) In the present study, no scaling factor was applied/necessary.

Table 3: Normalised mean square error (NMSE), fractional bias (FB) and correlation (*r*) for the spatially-varying observed climatology and modelled flash rates shown in Figure 3.

10

Flash-rate scheme	NMSE			FB			Spatial correlation (*r*)		
	Globe	Land	Ocean	Globe	Land	Ocean	Globe	Land	Ocean
Run 1 (PR92)	4.52	1.63	164.92	0.44	0.27	1.84	0.72	0.74	0.41
Run 2 (TS1)	3.66	1.66	6.77	0.13	0.18	-0.06	0.72	0.74	0.38
Run 3 (TS2)	3.63	1.65	6.92	0.21	0.28	-0.06	0.72	0.74	0.38
Run 4 (Mi99)	3.44	1.63	6.68	0.17	0.30	-0.30	0.72	0.74	0.39

3.7 Modelled LNO$_x$ and verification

3.7.1 Global LNO$_x$

The modelled global lightning-generated NO$_x$ using the various lightning flash-rate schemes are presented in Table 4. With

15 the new flash-rate parameterisations (Run 2), the modelled global LNO$_x$ increases to 6.6 Tg N yr^{-1} from 4.8 Tg N yr^{-1} for Run 1, an increase of 38%, most of which is due to the change in the oceanic flash-rate component. Of the total global LNO$_x$, about 20% is generated over the ocean in Run 2, compared to ~ 1% in Run 1. The partitioning into NH and SH is almost equal for both schemes. The Run 3 and Run 4 total LNO$_x$ emissions are similar to the Run 2 value. Given the same value of NO emitted per flash used for both IC and CG flashes, the partitioning of the global LNO$_x$ into NH, SH, and Land and Ocean

20 for all Runs in Table 4 is very similar to the partitioning of flash rate for the corresponding Runs in Table 1.

.

Table 4: Modelled global lightning-generated NOₓ using various lightning flash-rate schemes (Tg N yr⁻¹).

Flash-rate scheme	Lightning generated NO_x (Tg N yr^{-1})				
	Global	NH	SH	Land	Ocean
Run 1 (PR92)	4.84	2.39	2.45	4.79	0.05
Run 2 (TS1)	6.61	3.41	3.20	5.27	1.34
Run 3 (TS2)	6.11	3.14	2.97	4.77	1.34
Run 4 (Mi99)	6.39	3.40	2.99	4.69	1.70

The amount of global LNO_x produced, L_G (Tg N yr^{-1}), is a function of the global average flash rate, f_s (flash s^{-1}), and the

5   moles of NO produced per flash, P_{NO}:

$$L_G = 441.5 \times 10^{-6} \, f_s . P_{NO}, \qquad (21)$$

If the climatological average $f_s = 46.5$ flash s^{-1} based on the LIS/OTD satellite data is used, then

$$L_G = 20.5 \times 10^{-3} \, P_{NO}. \qquad (22)$$

The values in Table 4 are consistent with Eq. (21) when $P_{NO} = 330$ moles NO per flash as used in ACCESS-UKCA and the

modelled f_s from Table 1 are substituted. These values can be compared with a global estimate of $L_G = 5 \pm 3$ Tg N yr^{-1} based

on Schumann and Huntrieser's (2007) review. More recently, there have been estimates of LNO_x incorporating top-down

10   approaches, which we divide into (a) verification studies using other constraints and (b) model experiments.

Verification studies include: Using a CTM representing the LIS/OTD flash data, Martin et al. (2007) obtained an estimate of

6 ± 2 Tg N yr^{-1} that best reproduced satellite observations of tropospheric NO_2, O_3 and HNO_3. Miyazaki et al. (2014)

obtained $L_G = 6.3 \pm 1.4$ Tg N yr^{-1} and an average production of 310 moles NO per flash using an assimilation of multiple

satellite measurements of NO_2, O_3, HNO_3 and CO, and the LIS/OTD flash data into a global CTM. The global values for

15   Runs 2–4 in Table 4 compare very well with the above constrained estimates, considering their differences in NO per flash

used (the ratio $L_G/P_{NO} \approx 0.02$ in these estimates as per Eq. (22)). Using upper tropospheric airborne observations of LNO_x

and global satellite-retrieved tropospheric NO_2 column densities along with GEOS-Chem, Nault et al. (2017) estimated 665

moles NO per flash with global LNO_x at ~ 9 Tg N yr^{-1}.

Boersma et al. (2005) analysed above-cloud tropospheric NO_2 column retrievals from the GOME satellite observations for

20   the year 1997 for cloudy scenes over tropical oceans and continents, and found that the above-cloud annual-mean NO_2

Atmospheric
Chemistry
and Physics
Discussions
Open Access
EGU

column increases sharply with convective cloud-top height (H)—as $H^{5.1}$ for continents and $H^{4.6}$ for oceans, where $H > 6.5$ km. Considering that these above-cloud NO_2 columns primarily consist of contributions from lightning-generated NO_x, which is a direct function of flash rate, there is a very good agreement between these power-law exponents and those in the flash-rate relationships (11) and (18) for continents, and (20) for oceans. The analysis of Boersma et al. (2005) demonstrates

5   that the exponent of 1.73 in the PR92 oceanic flash-rate relationship (15) is unrealistic.

Model experiments include: Using a 3-D cloud resolving model coupled with observations from a thunderstorm and assuming $P_{NO} = 360$ moles NO per flash, Ott et al. (2007) estimated a global LNO_x of 7 Tg N yr^{-1}. Using a CTM constrained by the LIS/OTD flash together with a production of 500 moles NO per flash for all extratropical lightning north of 23°N in America and 35°N in Eurasia, and 260 moles NO per flash for the rest of the globe, Murray et al. (2012)[2] determined a

10   global LNO_x of 6 ± 0.5 Tg N yr^{-1}.

The modelled mean global distributions of LNO_x from the two runs presented in Figure 6a and b are essentially in proportion to the flash density distributions given in Figure 5c and Figure 5d, respectively. The new flash-rate parameterisations (Run 2) leads to a larger and broader distribution of LNO_x over the ocean compared to the PR92 scheme, and the former agrees better with the annual LNO_x distribution obtained by Miyazaki et al. (2014) (Figure 6c) with data assimilation.
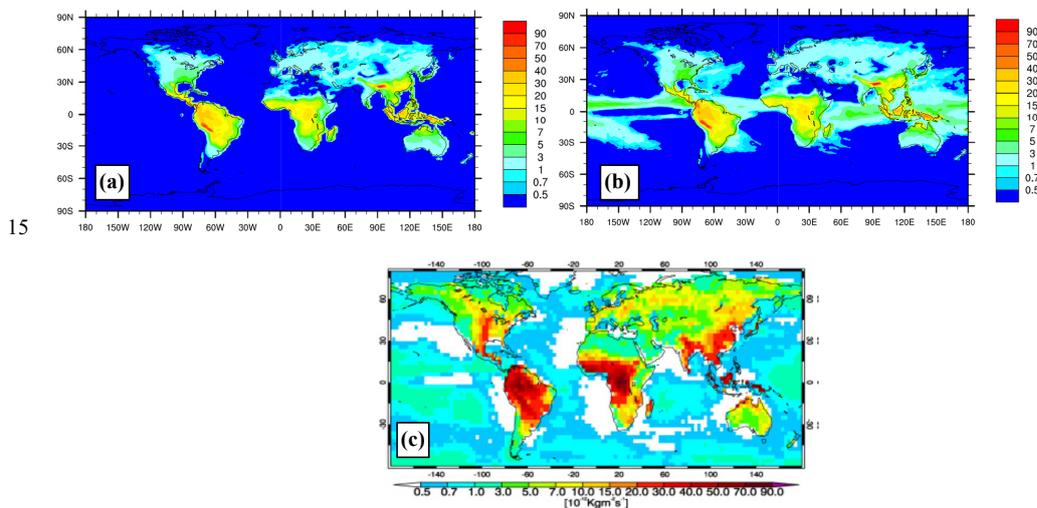
Figure 6: Global distribution of the annual-averaged LNO_x (10^{-12} kg N m^{-2} s^{-1}) for the year 2006: (a) model simulation with the default PR92 flash-rate parameterisations (Run 1), (b) model simulation with the new flash-rate parameterisations from this study (Run 2), and (c) the distribution obtained by Miyazaki et al. (2014, https://acp.copernicus.org/articles/14/3277/2014/) using
20   **assimilation of multiple satellite datasets into a global CTM. The respective global LNO_x totals are 4.8, 6.6 and 6.3 Tg N yr^{-1}.**

---

[2] In Murray et al. (2012), these production values are given as N per flash, but a cross-referencing suggests that these should be in NO per flash.

22

3.7.2 Vertical distribution

The vertical distribution of LNO_X in the model at a grid point location is a parameter (see Section 2.1) that is essentially unconstrained by observations. Figure 7 presents the modelled average vertical distribution of percentage of LNO_x mass in each 1-km layer for (a) tropical continental, (b) tropical marine, (c) midlatitude continental, and (d) subtropics regimes. Also

5   shown for comparison are the average profiles based on thunderstorm cases simulated by Pickering et al. (1998) using a 2-D convective cloud-resolving tracer transport model and those by Ott et al. (2010) using a 3-D convective cloud-resolving chemical transport model, with both studies using parameterised lightning. The profiles of Pickering et al. (1998) show peaks near the surface, as significant mass is transported to the boundary layer by downdrafts, and in the upper troposphere (the so-called 'C-shaped' profile), whereas those by Ott et al. (2010) show very little LNO_x mass in the boundary layer with the

10   majority of LNO_x remaining in the middle and upper troposphere (the so-called 'backward C-shaped' profile) where it is originally produced. Our model profiles match better with the Ott et al. (2010) profiles, but it gives an almost uniform distribution of LNO_x mass below 5 km whereas the latter decrease to almost zero. There is not a large difference between the modelled profiles for the various regimes, except that the tropical ones are almost uniformly distributed between 5 km and 12 km whereas the midlatitude and subtropical ones show a peak at 6.5 km. There are no direct measurements to verify any

15   of the LNO_x profiles.

In our model, once the amount of LNO_x at a grid point location at a model time step (60 min) has been computed, it is distributed evenly in the vertical in log-pressure coordinates from 500 hPa to the cloud top for IC flashes, and from surface to 500 hPa for CG flashes. The non-uniform model distribution in Figure 7 is largely caused by the averaging of the LNO_x profile from every time step over spatial and temporal variations in the cloud-top height.
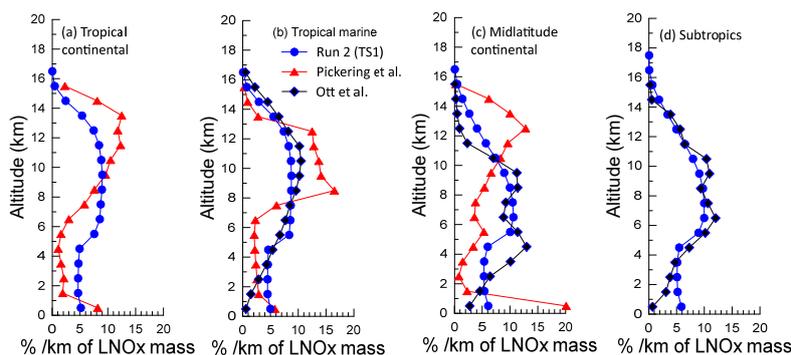
20

Figure 7: Average vertical distribution of percentage of LNO_x mass per kilometre for (a) tropical continental, (b) tropical marine, (c) midlatitude continental, and (d) subtropics regimes. The total LNO_x for these regimes calculated using the model Run 1 (PR92) is 3.69, 0.035, 1.09 and 0.74 Tg N yr^{-1} respectively, whereas that calculated using Run 2 (TS1) is 4.10, 1.09, 1.16 and 0.92 Tg N yr^{-1}

25   **respectively. The vertical profiles from Pickering et al. (1998) and Ott et al. (2010) are also shown (where available).**

3.7.3 Tropospheric NO₂ verification

As lightning impacts atmospheric NO_x directly, the changes in the modelled tropospheric NO_x can be examined and compared with observations. We use data from the global reanalysis of atmospheric composition produced by the Copernicus Atmosphere Monitoring Service (CAMS) (Inness et al., 2019; https://ads.atmosphere.copernicus.eu/cdsapp#!/dataset/cams-global-reanalysis-eac4-monthly) for comparison with the monthly-averaged modelled NO_2. The reanalysis was produced by assimilating space observations of aerosols and reactive gases using a 4D-Var method in an ECMWF global atmospheric model with 60 pressure levels (from 1000 to 1 hPa) and a horizontal resolution of 0.75° × 0.75°. For NO_2, the model assimilated the tropospheric column retrievals from the SCIAMACHY, OMI, and GOME-2 satellite overpasses at ~ 10:00 local time (LT), 13:30 LT and 09:30 LT, respectively (for the year 2006, only SCIAMACHY and OMI data were available for assimilation). Monthly-averaged total vertical column NO_2 reanalysis data (version - ECMWF Atmospheric Composition Reanalysis 4) are available and used here as follows.

The CAMS total NO_2 columns (N_v) are converted to tropospheric columns $N_{v,trop}$ by subtracting the total NO_2 columns over the Pacific (180°W) ($N_{v,180}$) from the NO_2 columns at all longitudes. This is a common approach used with the satellite data to separate the tropospheric and stratospheric amounts (Inness et al., 2019), and assumes a longitudinal homogeneity of the stratospheric NO_2 column amounts (uncertainty $< 1 \times 10^{15}$ molecules cm⁻²) and a constant and negligibly small tropospheric NO_2 column amounts over the reference 180°W longitude ($N_{v,trop,180}$) (uncertainty $< 0.5 \times 10^{15}$ molecules cm⁻²) (Lauer et al., 2002). Thus

$$N_{v,trop} = N_v - N_{v,180} + N_{v,trop,180}, \qquad (23)$$

where $N_{v,trop,180} \approx 0$. In Figure 8, we plot $N_{v,trop,180}$ for the year 2006 obtained from the model Runs 1 and 2. While these modelled values are smaller or comparable to the limit of above uncertainty value, they are neither constant nor negligibly small compared to the $N_{v,trop}$ (as shown below) and would reflect contributions from sources such as lightning, aviation, shipping, and possibly regional transport. It is also clear in Figure 8 that the column amounts are higher for Run 2 within the latitudes ± 30° mainly due to higher flash rates over the ocean.
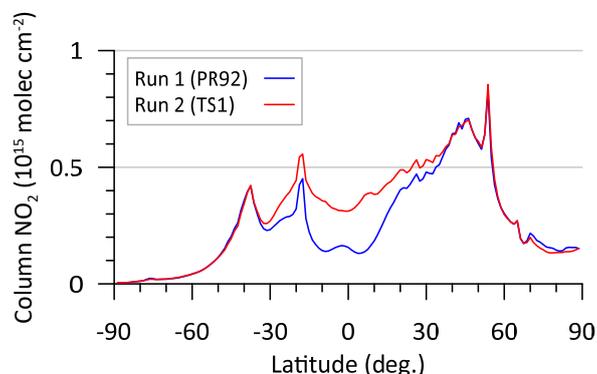
Figure 8: Mean tropospheric NO2 column amounts (in units 10^{15} molecules cm^{-2}) over the reference longitude (180°W) ($N_{v,trop,180}$) for the year 2006 obtained from the model Run 1 (default PR92 flash-rate parameterisations) and Run 2 (new flash-rate parameterisations from this study).

5

As $N_{v,trop,180}$ is not available from the satellite data as it is implicitly neglected, we take the average of the two curves in Figure 8 (so as to not to bias the results either way) and use it in Eq. (23) to determine $N_{v,trop}$ from the CAMS data. The modelled and CAMS zonal annual-mean $N_{v,trop}$ for the globe are presented in Figure 9a. The two model simulations differ primarily within the tropics, with the new lightning flash-rate parameterisations yielding ~ 15% larger values compared to

10 the default setup. The global model variations agree very well with the CAMS data, showing a peak in the industrialised Northern Hemisphere dominated by surface NO$_2$ emissions. In Figure 9b for the ocean, the agreement with the data is again very good, but it is apparent that the CAMS NO$_2$ is better simulated by the model with the new oceanic flash rate within the tropics than with the PR92 oceanic flash-rate parameterisation, whereas the two model curves are almost the same for the other latitudes. For land (Figure 9c), the two model curves are nearly identical, with the model overestimating the CAMS

15 NO$_2$ column amounts in the southern tropical region. The results in Figure 9 demonstrate that the use of the new oceanic flash-rate improves the tropospheric NO$_2$, and they also imply that the value 330 moles NO per flash used is appropriate, except perhaps a slightly lower value over land in the southern tropic. Obviously, there are uncertainties associated with the CAMS reanalysis and the assimilated satellite columns, which are documented in the appropriate references cited above, as well as those associated with model inputs (e.g. emissions) and processes.
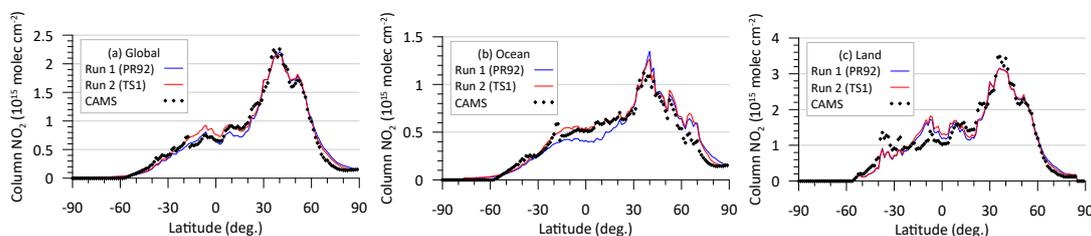
20

Figure 9: Zonal annual-mean tropospheric NO₂ column ($N_{v,trop}$) (in units 10^{15} molecules cm⁻²) modelled using the default PR92 parameterisations (Run 1), the new lightning flash-rate parameterisations from this study (Run 2), and the CAMS reanalysis data for the year 2006 over (a) globe, (b) ocean and (c) land.

In Table 5 for latitudes between ± 30°, the performance measures show a good improvement in the simulation of the reanalysis NO₂ columns with Run 2 (TS1) over the default scheme Run 1 (PR92) for the ocean, but for land there is a very slight deterioration in the performance.

Table 5: Normalised mean square error (NMSE), fractional bias (FB) and correlation (r) for the observed and modelled NO₂ columns shown in Figure 9 for latitudes between ± 30°.

Flash-rate scheme	NMSE			FB			Correlation (r)		
	Globe	Land	Ocean	Globe	Land	Ocean	Globe	Land	Ocean
Run 1 (PR92)	0.019	0.040	0.040	0.073	-0.013	0.162	0.94	0.78	0.88
Run 2 (TS1)	0.017	0.047	0.006	-0.044	-0.064	-0.039	0.93	0.75	0.95

4 Impact on tropospheric composition

We present the impact of LNOₓ determined from the flash-rate parameterisations from Runs 1 and 2 on tropospheric composition.

4.1 Oxides of nitrogen (NOₓ)

The modelled tropospheric NO₂ columns and their comparison with observations have already been presented in Section 3.7.3. Figure 10 presents the zonal distribution of NOₓ (as NO₂) from the two model simulations and the difference between the two. In the lower troposphere, the two modelled distributions of the zonal annual-mean NOₓ (as NO₂) are virtually

26

identical, with highest levels predicted within latitudes 20–60º N. These levels are governed by surface emissions of NO_x which are the same in both simulations. The secondary concentration maximum at ~15 km is due to the lightning-generated NO_x. The new lightning parameterisations cause an increase in the mid- to upper-tropospheric NO_x (Figure 10c), particularly within the tropics and subtropics, and this increase is by as much as 40 ppt in the northern tropics.

5 Overall, the increase in the volume-weighted global tropospheric NO_x is by 8.7 ppt (15.7%), and it is by 9.9 ppt (28.0%) over the ocean and by 6.3 ppt (6.7%) over land.
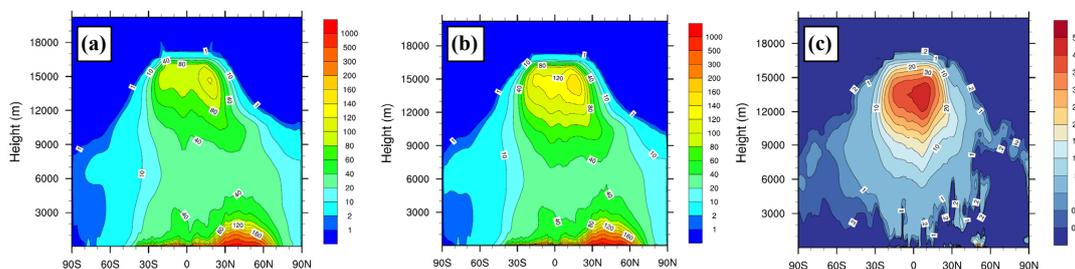
Figure 10: Zonal annual-mean tropospheric NO_x (as NO_2, pptv) modelled using (a) the default PR92 parameterisations (Run 1)
10 **and (b) the new lightning flash-rate parameterisations from this study (Run 2). The difference between Run 2 and Run 1 is shown in (c).**

4.2 Ozone (O_3)

Tropospheric ozone is a by-product of the oxidation of carbon monoxide (CO), CH_4 and other volatile organic compounds in
15 the presence of NO_x and is thus impacted by LNO_x.

With the new flash-rate parameterisations (Run 2), the modelled tropospheric O_3 burden increases from 284 to 308 Tg O_3, a rise of 8.5% over the default PR92 scheme (Run 1). The new burden is closer to a the ACCMIP (Atmospheric Chemistry and Climate Model Intercomparison Project) multi-model mean of 337 ± 23 Tg O_3 reported by Young et al. (2013), the latter value is consistent with measurement climatologies (this, however, does not necessarily mean that LNO_x in these models is
20 represented correctly). The Run 3 and Run 4 ozone burdens are 306 and 308 Tg, respectively.

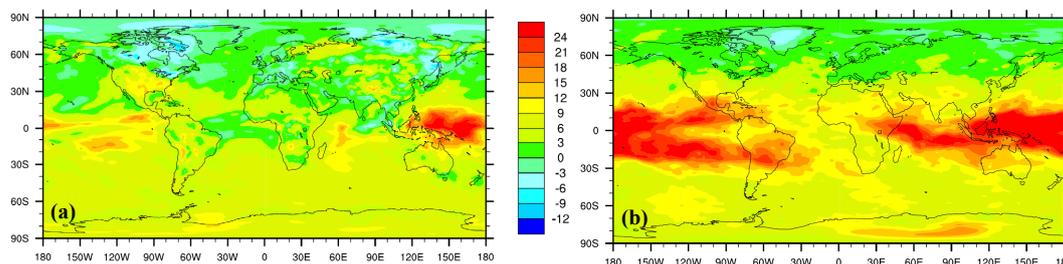The mean relative difference (%) between the global ozone mixing ratios predicted using the new lightning flash-rate parameterisations and the default PR92 parameterisations is shown in Figure 11. Near the surface (Figure 11a), there are significant increases in ozone over the tropical oceans, especially in the Pacific and western Indian Ocean, and in most of the Southern Hemisphere (roughly by 8% on average). Over land, there are regions (e.g. south-eastern U.S.A. and northern

27

Australia) where ozone has increased, and there are a few regions in the mid to high latitudes in the Northern Hemisphere where ozone has decreased very slightly. At an altitude of 6400 m (~ 450 hPa) (Figure 11b), there are even bigger increases in global ozone using the new flash-rate parameterisations, particularly in the tropics, by as much as 25%, and in the Southern Hemisphere. This is because most LNO_x emissions occur in the middle to upper tropical troposphere where the

5   photochemical production of ozone is most efficient.

Figure 11: Mean relative difference (%) between the global ozone mixing ratios predicted by Run 2 using the new lightning flash-rate parameterisations from this study and the default PR92 parameterisations (Run 1): (a) at 20 m (the lowest model level) and
10   **(b) at 6400 m (~ 450 hPa).**

In Figure 12, we compare the modelled monthly averaged ozone with ground-based in-situ observations from the World Data Centre for Reactive Gases (GAW-WDCRG, http://ebas.nilu.no; https://www.gaw-wdcrg.org;) for the year 2006 at five stations. The site selection was based on these sites being either oceanic or coastal along with data availability. The sites are
15   Ushuaia (54.85ºS, 68.31ºW), Cape Grim (40.68ºS, 144.69ºE), Mauna Loa (19.54ºN, 155.58ºW), Minamitorishima (24.29ºN, 153.98ºE), and Mace Head (53.33ºN, 9.90 ºW), which cover a range of latitudes. The hourly data were averaged to monthly values, and only those observational months were considered for which there were more than 75% valid hourly data points. The model simulates the observed monthly variation well, at least qualitatively. While the new flash-rate parameterisations do not fully explain the differences between the modelled variation and the observed one, particularly at Mauna Loa and
20   Mace Head, overall there is a slight improvement in the correlation coefficient (*r*) and normalised mean square error (NMSE) with the new parameterisations over the PR92 scheme at all sites, which in turn suggests a slight improvement in the prediction of seasonal variation of ground-level ozone and its magnitude.
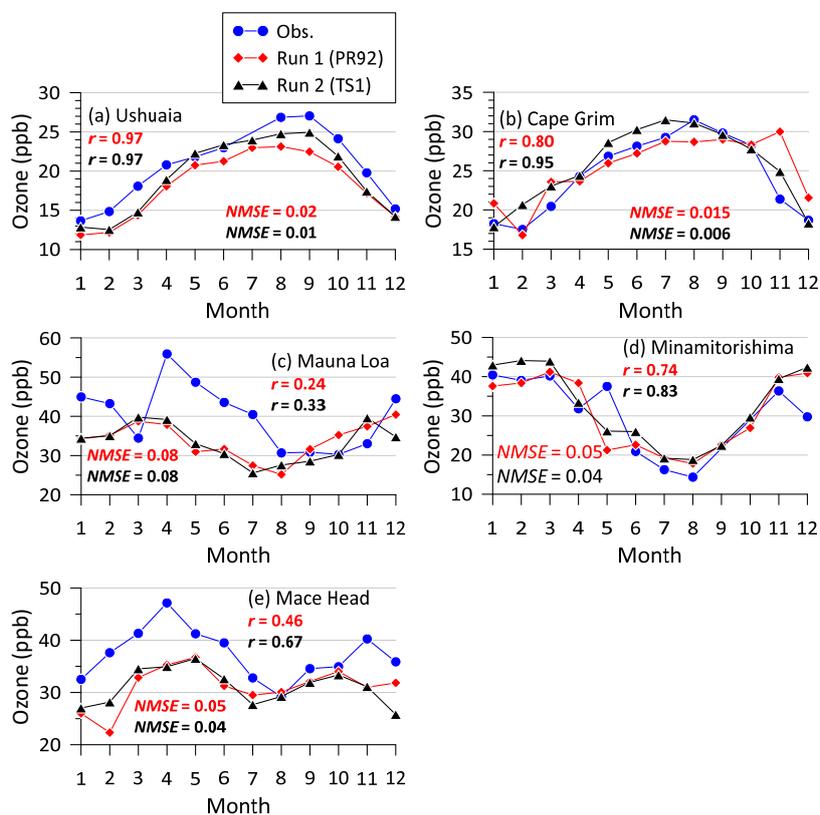
25

Figure 12: Comparison of the modelled monthly-averaged ozone concentrations with observations at five oceanic/coastal ground stations for the year 2006. The two model runs are with the (a) default PR92 parameterisations (Run 1) and (b) new lightning flash-rate parameterisations (Run 2, this study). The values of correlation coefficient (*r*) and normalised mean square error (NMSE) are also shown.

The modelled zonal annual-mean tropospheric O_3 from the two Runs and the difference between the two are presented in Figure 13. In the lower troposphere, the modelled ozone is smaller over the Southern Hemisphere than over the Northern Hemisphere (Figure 13a and Figure 13b). The new flash-rate parameterisations result in O_3 increases everywhere (Figure 13c). Closer to the surface, the increase is approximately 2 ppb (by volume) in the Southern Hemisphere and 0.5–2 ppb in the Northern Hemisphere. The largest increases are nearly 8 ppb in the tropics at altitudes ~ 9 km.

29
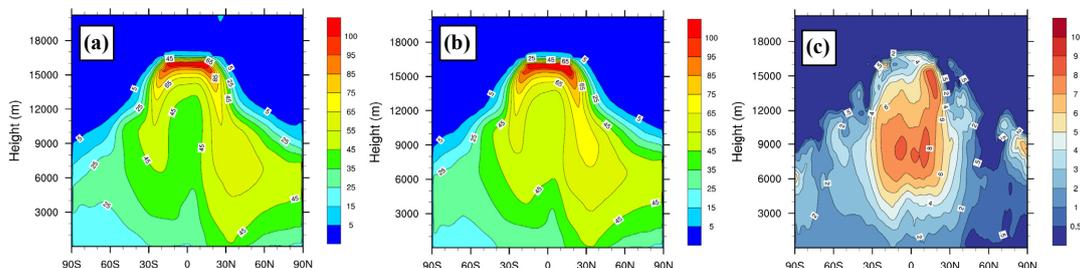
Figure 13: Zonal annual mean tropospheric ozone (ppbv) modelled using (a) the default PR92 parameterisations (Run 1) and (b) the new lightning flash-rate parameterisations from this study (Run 2). The difference between Run 2 and Run 1 is shown in (c).

5   The modelled zonal ozone distribution can be compared with observations. We use the monthly mean vertical ozone profile data for the year 2006, given as zonal means, from the publicly-available Bodeker Scientific database (http://www.bodekerscientific.com/data/monthly-mean-global-vertically-resolved-ozone) which combines measurements from several satellite-based instruments and ozone profile measurements from the global ozone-sonde network. The database spans the period 1979 to 2016 with 5° latitude resolution and 70 altitude levels (1 to 70 km). Different 'Tiers' of data are

10   provided, and we used the highest Tier 1.4 (vn1.0) data. For comparison with the model predictions, these monthly profile data were regridded to the model resolution. The modelled monthly tropospheric mask was zonal averaged and then applied to the monthly regridded data.

There is an agreement, both in magnitude and distribution, between the modelled zonal ozone in Figure 13a and b, and the data plotted in Figure 14a. The model reproduces the observed lower levels of tropospheric ozone in the Southern

15   Hemisphere. The observed high levels just below the tropopause within 10–40ºN are somewhat better reproduced by the new flash-rate parameterisations. Figure 14b and c represent the differences between the modelled and observed ozone for the PR92 scheme and the new parameterisations, respectively. Overall, the model underestimation in the Southern Hemisphere has reduced with the new parameterisations. In the Northern Hemisphere, the new scheme tends to overestimate ozone within 10–50 ºN below ~ 9 km the Northern Hemisphere, but with a slight improvement for higher latitudes. Obviously,

20   there are additional factors that influence tropospheric ozone distribution in the model, such as dynamics, including inter-hemispheric mixing and stratosphere-to-troposphere exchange, and how chemical mechanisms are represented. However, it is evident that the new flash-rate parameterisations lead the modelled ozone closer to the observations. Getting ozone in the upper troposphere correct is climatically important as surface temperature is more sensitive to changes in ozone in the upper troposphere and near the tropopause than those in the lower atmosphere (Forster and Shine, 1997) and, similarly, radiative

25   forcing due to tropospheric ozone is more sensitive to ozone abundance in the upper troposphere (Worden et al., 2011).

Overall, the increase in the volume-weighted global tropospheric O_3 is by 4.1 ppb (8.0%), and it is by 4.4 ppb (9.1%) over the ocean and by 3.6 ppb (6.3%) over land.
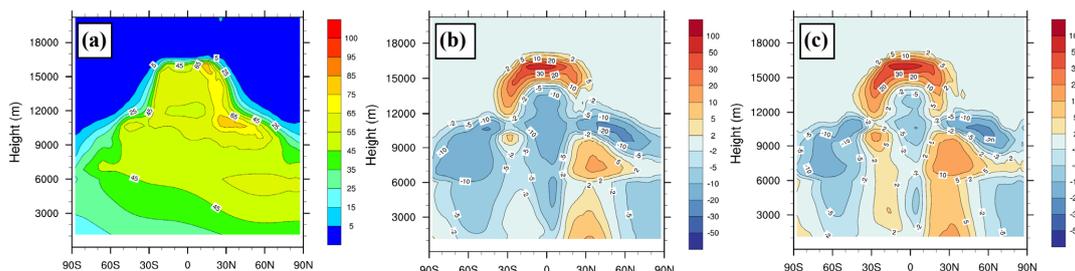
Figure 14: Zonal distribution of ozone concentration (ppbv) for the year 2006: (a) observed distribution based on the global monthly mean vertical ozone profile database available from http://www.bodekerscientific.com; (b) the difference between the concentration modelled using the default PR92 lightning parameterisations (Run 1) and the observations; and (c) the difference between the concentration modelled using the new lightning parameterisations (Run 2) and the observations.

4.3 Hydroxyl (OH) radical

The hydroxyl radical (OH) is the dominant oxidizing (and cleansing) agent in the global troposphere and controls the atmospheric abundance and chemical lifetime of most natural and anthropogenic gases, such as methane (CH_4). The tropospheric abundance of OH is determined by a complex series of chemical reactions involving tropospheric ozone, methane, carbon monoxide (CO), non-methane volatile organic compounds (NMVOCs), and NO_x, and also the amount of solar radiation and humidity (Naik et al., 2013). Through these reactions, the amount of LNO_x produced also impacts OH.

The modelled zonal annual mean tropospheric OH in Figure 15 shows highest OH concentrations near the surface in the tropics, with values as high as $(25 - 30) \times 10^5$ molecules cm^{-3} at ~ 20º N. The concentrations decrease with altitude, but there is a secondary maximum in the upper troposphere at around 13 km. There is an increase in the OH concentration using the new flash-rate parameterisations (Figure 15c), particularly in the upper troposphere in the tropics, by as much as 5×10^5 molecules cm^{-3}.
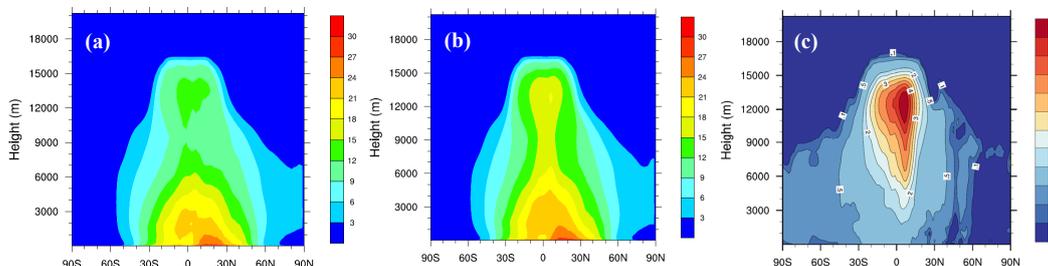
Figure 15: Zonal annual mean tropospheric OH (× 10⁵ molecules cm⁻³) modelled using (a) the default PR92 parameterisations (Run 1) and (b) the new lightning flash-rate parameterisations from this study (Run 2). The difference between Run 2 and Run 1 is shown in (c).

5

The annual mean relative OH difference (%) between Run 2 and Run 1 near the surface (Figure 16a) shows an increase in OH over the Southern Hemisphere oceans and Antarctica, and pockets of increase and slight decrease in the Northern Hemisphere. At mid-troposphere, at a model height of 6.4 km (~ 450 hPa) (Figure 16b), there are large areas showing an increase in OH by up to 20–25% with the new flash-rate parameterisations, particularly in the tropics and Southern

10 Hemisphere.
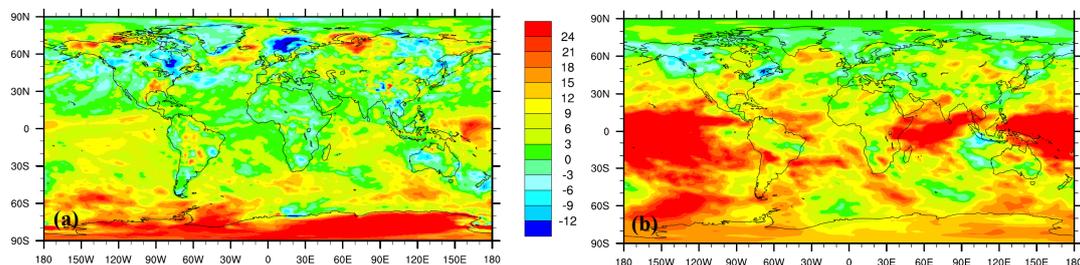
Figure 16: Mean relative difference (%) between the hydroxyl radical (OH) predicted using the new lightning flash-rate parameterisations (Run 2) and the default PR92 parameterisations (Run 1): (a) at 20 m (the lowest model level) and (b) at 6400 m (~ 450 hPa).

15

Overall, we find that, with the new flash-rate parameterisations, there is a 13% increase in the annual-average volume-weighted global tropospheric OH, from 10.6×10^5 to 12.0×10^5 molecules cm⁻³. The increase over the ocean is by 1.6×10^5 (16.3%) and that over land by 0.9×10^5 molecules cm⁻³ (7.6%). The global amount can be compared with the ACCMIP multi-model mean of $11.1 \pm 1.6 \times 10^5$ molecules cm⁻³ derived by Naik et al. (2013) for the year 2000. Recent observational

20 values reported by Wolfe et al. (2019) for August are $12.6 \pm 2.9 \times 10^5$ for the Northern Hemisphere and $8.1 \pm 1.9 \times 10^5$ for

32

the Southern Hemisphere, and these for February are $8.8 \pm 2.1 \times 10^5$ and $11.4 \pm 2.8 \times 10^5$, respectively. These can be compared with the corresponding modelled values 16.9, 7.3, 8.0 and 11.6×10^5 using the PR92 scheme, and 18.7, 8.5, 9.2 and 13.5×10^5 using the new scheme. Clearly, the model value in the Northern Hemisphere in August is considerably larger than the observation even with the PR92 scheme. It is known that the UKCA StratTrop configuration yields substantially larger OH in the Northern Tropics at low altitudes compared to observations and to the ACCMIP multi-model estimates (Archibald et al., 2020).

With an overall increase in OH using the new flash-rate parameterisations in ACCESS-UKCA, the global annual mean lifetime of CH$_4$ against loss by tropospheric OH (τ_{CH4_OH}, defined as the division of the global total atmospheric CH$_4$ burden and the globally integrated CH$_4$ loss rate by reaction with tropospheric OH) decreases by 6.7%, from 7.5 to 7.0 years.

4.4 Carbon monoxide (CO)

There is a decrease in the modelled tropospheric carbon monoxide (CO) with the use of the new lightning parameterisations, as evident from the zonal annual-mean difference plot in Figure 17 (this CO reduction is coupled to the OH increase, via the reaction OH + CO → CO$_2$ + H). In the lower troposphere, the decrease is by approximately 4–6 ppb (~ 7%) in the Southern Hemisphere and 2–4 ppb (~ 3%) in the Northern Hemisphere. This reduction gets a little larger in the mid to upper troposphere in the tropics. Overall, the reduction in the volume-weighted global CO is by 4.5 ppb (5.6%). Over the ocean is by 4.7 ppb (6.2%) and that over land by 4.0 ppb (4.5%).
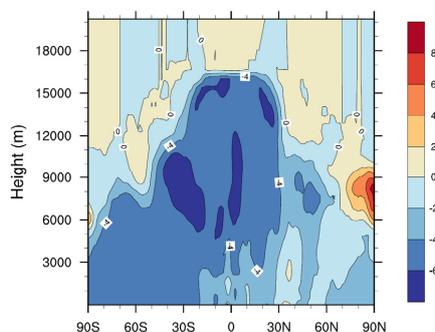

Figure 17: The difference between the zonal annual-mean tropospheric CO (ppbv) modelled using the new lightning flash-rate parameterisations (Run 2) and the default PR92 parameterisations (Run 1).

In Figure 18, we compare the modelled monthly-averaged CO with surface flask observations from the same GAW-WDCRG sites as in Figure 12 (data from Minamitorishima were missing for 4 months, so are not presented). The model is

in qualitative agreement with the data, but generally the differences between the model runs are substantially smaller than the model-data differences. The NMSE and *r* values suggest a mixed result.
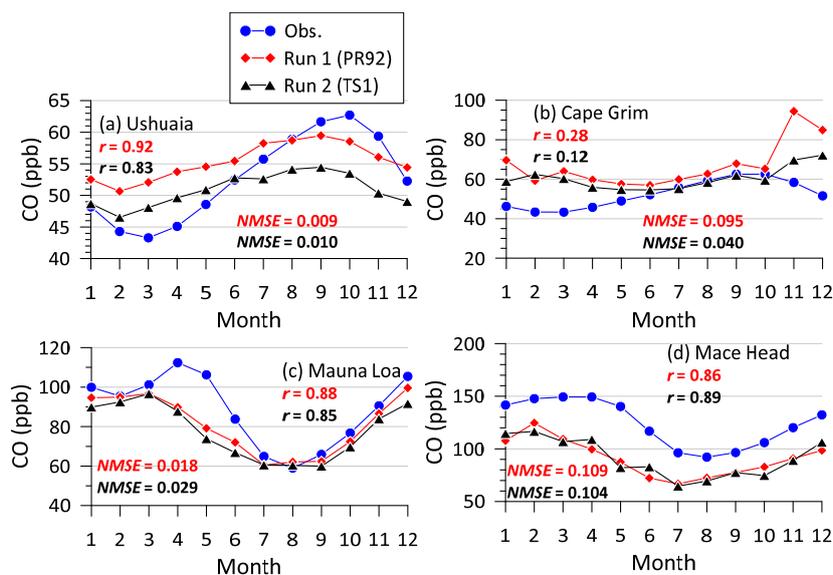
Figure 18: Comparison of the modelled monthly-averaged CO concentrations (ppbv) with observations at four oceanic/coastal ground stations for the year 2006. The two model runs are with the (a) default PR92 parameterisations (Run 1) and (b) new lightning flash-rate parameterisations (Run 2). The values of correlation coefficient (*r*) and normalised mean square error (NMSE) are also shown.

5 Conclusions

We have critically examined parameterisations of lightning flash rate that are based on the cloud-top height approach. Testing of the widely used Price and Rind (1992) (PR92) parameterisations within the ACCESS-UKCA global chemistry-climate model for the year 2006 using the global LIS/OTD satellite data has revealed that while the parameterisation for land yields satisfactory predictions, with a globally averaged flash rate of 31.03 flashes s^{-1} compared to the observed 34.92 flashes s^{-1}, the oceanic parameterisation severely underestimates the observed flash rate, yielding on average 0.33 flashes s^{-1} compared to the observed 9.16 flashes s^{-1}. This leads to lightning-generated NO_x (LNO_x) being underestimated proportionally over the ocean and thus influencing tropospheric composition.

Following Boccippio's (2002) scaling relationships between thunderstorm electrical generator power and storm geometry as the basis, we derived alternative flash-rate parameterisations. While the new parameterisation for land performed slightly better than the corresponding PR92 one, giving a globally averaged flash rate of 34.23 flashes s^{-1} compared to the observed

34

34.92 flashes s^{-1}, the new parameterisation for ocean performed more accurately, giving a globally averaged flash rate of 8.84 flashes s^{-1} compared to the observed 9.16 flashes s^{-1}. We also tested an oceanic parameterisation by Michalon et al. (1999), which gives a global oceanic average of 11.31 flashes s^{-1}. With the new parameterisations, there was an increase in global LNO$_x$ from 4.8 to 6.6 Tg N yr^{-1}, with the new estimate comparable to 6.3 ± 1.4 Tg N yr^{-1} obtained by Miyazaki et al.

5 (2014) using an assimilation of multiple satellite datasets into a global CTM. The model's use of 330 moles NO produced per flash is consistent with the average value 310 moles NO per flash determined by Miyazaki et al. (2014).

The use of the new flash-rate parameterisations in ACCESS-UKCA demonstrated a considerable impact on the modelled tropospheric composition compared to the defaults PR92 parameterisations, mainly due to the change in the oceanic flash-rate component. In particular, the following impacts were observed:

10
- An increase in the mid- to upper-tropospheric NO$_x$ by as much as 40 ppt (as NO$_2$) in the northern tropics. An overall increase in the global NO$_x$ by 8.7 ppt (15.7%) and by 9.9 ppt (28.0%) over the ocean. A better agreement of the modelled tropospheric NO$_2$ columns with the CAMS reanalysis data.
- The tropospheric O$_3$ burden increased by 8.5%, from 284 to 308 Tg O$_3$, closer to a multi-model estimate of 337 ± 23 Tg O$_3$ (Young et al., 2013), the latter supported by measurement climatology. Overall, the distribution of the

15 modelled ozone in the troposphere improved compared to the global profile observations and ground stations data.
- A 13% increase in the annual-average volume-weighted global tropospheric OH, from 10.6 × 10^5 to 12.0 × 10^5 molecules cm^{-3}.
- A decrease in the global annual mean methane lifetime against loss by tropospheric OH by 6.7%.
- An overall reduction in the global CO by 4.5 ppb (5.6%).

20 The approach of parameterising lightning flash rate in terms of convective cloud-top height works well given its simplicity, and continues to be useful in accounting for LNO$_x$ in global models, although there were some significant spatial distributional differences in the modelled flash-rate density compared to the satellite data. The approach is also very sensitive due to an almost 5th power dependence on cloud-top height. With increased computational power in the future, it may be possible to understand and represent global LNO$_x$ in a better process-based manner through a cloud-resolving modelling

25 framework with an explicit prediction of the electrical activity in storms.

Recent global chemistry-climate modelling studies using flash-rate parameterisations based on the convective cloud-top height show an increase in LNO$_x$ emissions in a future warming climate (e.g., Banerjee et al. 2014; Clark et al., 2017; Iglesias-Suarez et al., 2018), primarily as a result of increases in the depth of convection. This is also the case with a CAPE and precipitation rate based parameterisation (Romps et al., 2014). Conversely, it is found that a flash-rate scheme based on

30 convective mass flux (Clark et al., 2017) and that based on upward cloud ice flux (Finney et al., 2018) predict a global decrease in future lightning flash density (under the RCP8.5 scenario). Clearly, there is an existing uncertainty as to which physical parameterisation approach best represents the reality and the feedbacks that are important for lightning under

climate change, although parameters such as cloud ice content and/or updraught mass flux used in flux-based lightning schemes are perhaps currently not well constrained by available observations.

Data availability

The ACCESS-UKCA global model output data (in NetCDF format) used for analysis and plotting, and the processed model
5 lighting and composition data (in ASCII format) used for comparison with observations can be made available by contacting the corresponding author (Ashok Luhar: ashok.luhar@csiro.au). The observational data used in the present study are available online, as indicated in the text.

Competing interests

The authors declare that they have no conflict of interest.

20

36

References

Abraham, N. L., Archibald, A. T., Bellouin, N., Boucher, O., Braesicke, P., Bushell, A., Carslaw, K. S., Collins, W., Dalvi, M., Emmerson, K. M., Folberth, G., Haywood, J., Johnson, C., Kipling, Z., Macintyre, H., Mann, G. W., Telford, P. J., Merikanto, J., Morgenstern, O., O'Connor, F., Ordonez, C., Osprey, S., Pringle, K. J., Pyle, J. A., Rae, J. G. L., Reddington,

5   C. L., Savage, D., Spracklen, D., Stier, P., and West, R.: Unified Model Documentation Paper No. 84 (http://www.ukca.ac.uk/images/b/b1/Umdp_084-umdp84.pdf): United Kingdom Chemistry and Aerosol (UKCA) Technical Description MetUM Version 8.4. UK Met Office, Exeter (UK), pp. 74, 2012.

Allen, D. J. and Pickering, K. E.: Evaluation of lightning flash rate parameterizations for use in a global chemical transport model, J. Geophys. Res., 107, 4711, doi:10.1029/2002JD002066, 2002.

10 Archibald, A. T., O'Connor, F. M., Abraham, N. L., Archer-Nicholls, S., Chipperfield, M. P., Dalvi, et al.: Description and evaluation of the UKCA stratosphere–troposphere chemistry scheme (StratTrop vn 1.0) implemented in UKESM1, Geosci. Model Dev., 13, 1223–1266, https://doi.org/10.5194/gmd-13-1223-2020, 2020.

Banerjee, A., Archibald, A. T., Maycock, A. C., Telford, P., Abraham, N. L., Yang, X., Braesicke, P., and Pyle, J. A.: Lightning NO$_x$, a key chemistry–climate interaction: impacts of future climate change and consequences for tropospheric

15 oxidising capacity, Atmos. Chem. Phys., 14, 9871–9881, https://doi.org/10.5194/acp-14-9871-2014, 2014.

Barthe, C., and Barth M. C.: Evaluation of a new lightning-produced NO$_x$ parameterization for cloud resolving models and its associated uncertainties, Atmos. Chem. Phys., 8, 4691–4710, https://doi.org/10.5194/acp-8-4691-2008, 2008.

Bi, D. H., Dix, M., Marsland, S. J., O'Farrell, S., Rashid, H. A., Uotila, P., Hirst, A. C., Kowalczyk, E., Golebiewski, M., Sullivan, A., Yan, H. L., Hannah, N., Franklin, C., Sun, Z. A., Vohralik, P., Watterson, I., Zhou, X. B., Fiedler, R., Collier,

20 M., Ma, Y. M., Noonan, J., Stevens, L., Uhe, P., Zhu, H. Y., Griffies, S. M., Hill, R., Harris, C., and Puri, K.: The ACCESS coupled model: description, control climate and evaluation, Australian Meteorological and Oceanographic Journal, 63, 41–64, 2013, http://www.bom.gov.au/amm/docs/2013/bi1.pdf.

Boccippio, D. J.: Lightning scaling relations revisited, J. Atmos. Sci., 59, 1086–1104, https://doi.org/10.1175/1520-0469(2002)059<1086:LSRR>2.0.CO;2, 2002.

25 Boersma, K. F., Eskes, H. J., Meijer, E. W., and Kelder, H. M.: Estimates of lightning NO$_x$ production from GOME satellite observations, Atmos. Chem. Phys., 5, 2311–2331, https://doi.org/10.5194/acp-5-2311-2005, 2005.

Butkovskaya, N., Kukui, A., and Le Bras, G.: HNO$_3$ Forming Channel of the HO$_2$ + NO Reaction as a Function of Pressure and Temperature in the Ranges of 72−600 Torr and 223−323 K, Phys. Chem. A, 111, 9047–9053, https://doi.org/10.1021/jp074117m, 2007.

Cecil, D. J., Buechler, D. E., and Blakeslee, R. J.: Gridded lightning climatology from TRMM-LIS and OTD: Dataset description, Atmos. Res., 135–136, 404–414, https://doi.org/10.1016/j.atmosres.2012.06.028, 2014.

Choi, Y., Wang, Y., Zeng, T., Martin, R. V., Kurosu, T. P., and Chance, K.: Evidence of lightning NO_x and convective transport of pollutants in satellite observations over North America, Geophys. Res. Lett., 32, L02805, doi:10.1029/2004GL021436, 2005.

Clark, S. K., Ward, D. S., and Mahowald, N. M.: Parameterization-based uncertainty in future lightning flash density, Geophys. Res. Lett., 44, 2893–2901, doi:10.1002/2017GL073017, 2017.

Dahlmann, K., Grewe, V., Ponater, M., and Matthes, S.: Quantifying the contributions of individual NO_x sources to the trend in ozone radiative forcing, Atmos. Environ., 45, 2860–2868, https://doi.org/10.1016/j.atmosenv.2011.02.071, 2011.

Dee, D. P., Uppala, S. M., Simmons, A. J., Berrisford, P., Poli, P., Kobayashi, S., Andrae, U., Balmaseda, M. A., Balsamo, G., Bauer, P., Bechtold, P., Beljaars, A. C. M., van de Berg, L., Bidlot, J., Bormann, N., Delsol, C., Dragani, R., Fuentes, M., Geer, A. J., Haimberger, L., Healy, S. B., Hersbach, H., Holm, E. V., Isaksen, L., Kallberg, P., Kohler, M., Matricardi, M., McNally, A. P., Monge-Sanz, B. M., Morcrette, J.-J., Park, B.-K., Peubey, C., de Rosnay, P., Tavolato, C., Thepaut, J.-N., and Vitarta, F.: The ERA-Interim reanalysis: configuration and performance of the data assimilation system, Q. J. Roy. Meteor. Soc., 137, 553–597, doi:10.1002/qj.828, 2011.

DeCaria, A. J., Pickering, K. E., Stenchikov, G. L., and Ott, L. E.: Lightning-generated NO_x and its impact on tropospheric ozone production: A three-dimensional modeling study of a Stratosphere-Troposphere Experiment: Radiation, Aerosols and Ozone (STERAO-A) thunderstorm, J. Geophys. Res., 110, 1–13, doi:10.1029/2004JD005556, 2005.

Deierling, W. and Petersen, W. A.: Total lightning activity as an indicator of updraft characteristics, Journal of Geophysical Research, 113, D16210, doi:10.1029/2007JD009598, 2008.

Emmons, L. K., Schwantes, R. H., Orlando, J. J., Tyndall, G., Kinnison, D., Lamarque, J.-F., et al.: The Chemistry Mechanism in the Community Earth System Model Version 2 (CESM2), Journal of Advances in Modeling Earth Systems, 12, e2019MS001882. https://doi.org/10.1029/2019MS001882, 2020.

Finney, D. L., Doherty, R. M., Wild, O., Huntrieser, H., Pumphrey, H. C., and Blyth, A. M.: Using cloud ice flux to parametrise large-scale lightning, Atmos. Chem. Phys., 14, 12665–12682, doi:10.5194/acp-14-12665-2014, 2014.

Finney, D. L., Doherty, R. M., Wild, O., and Abraham, N. L.: The impact of lightning on tropospheric ozone chemistry using a new global lightning parametrisation, Atmos. Chem. Phys., 16, 7507–7522, doi:10.5194/acp-16-7507-2016, 2016.

Forster, P. M. D. and Shine, K. P.: Radiative forcing and temperature trends from stratospheric ozone changes, J. Geophys. Res., 102(D9), 10,841–10,855, doi:10.1029/96JD03510, 1997.

Futyan, J. M. and Del Genio, A. D.: Relationships between lightning and properties of convective cloud clusters, Geophysical Research Letters, 34, L15705, https://doi.org/10.1029/2007GL030227, 2007.

Gordillo-Vázquez, F. J., Pérez-Invernón, F. J., Huntrieser, H., and Smith, A. K.: Comparison of six lightning parameterizations in CAM5 and the impact on global atmospheric chemistry, Earth and Space Science, 6, 2317–2346,
5   https://doi.org/10.1029/2019EA000873, 2019.

Gregory, D. and Rowntree, P. R.: A mass flux convection scheme with representation of cloud ensemble characteristics and stability-dependent closure, Mon. Weather Rev., 118, 1483–1506, doi:10.1175/1520-0493(1990)118<1483:AMFCSW>2.0.CO;2, 1990.

Grewe, V.: Impact of climate variability on tropospheric ozone, Sci. Total Environ., 374, 167–181,
10   doi:10.1016/j.scitotenv.2007.01.032, 2007.

Gultepe, I. and Isaac, G. A.: Aircraft observations of cloud droplet number concentration: Implications for climate studies, Q. J. R. Meteorol. Soc., 130, 2377–2390, doi: 10.1256/qj.03.120, 2004.

Hardiman, S. C., Boutle, I. A., Bushell, A. C., Butchart, N., Cullen, M. J. P., Field, P. R., Furtado, K., Manners, J. C., Milton, S. F., Morcrette, C., O'Connor, F. M., Shipway, B. J., Smith, C., Walters, D. N., Willett, M. R., Williams, K. D.,
15   Wood, N., Abraham, N. L., Keeble, J., Maycock, A. C., Thuburn, J., and Woodhouse, M. T.: Processes controlling tropical tropopause temperature and stratospheric water vapor in climate models, J. Climate, 28, 6516–6535, doi:10.1175/JCLI-D-15-0075.1, 2015.

Hudman, R. C., Jacob, D. J., Turquety, S., et al.: Surface and lightning sources of nitrogen oxides over the United States: Magnitudes, chemical evolution, and outflow, J. Geophys. Res., 112, D12S05, doi:10.1029/2006JD007912, 2007.

20   Huntrieser, H., Schumann, U., Schlager, H., Höller, H., Giez, A., Betz, H.-D., Brunner, D., Forster, C., Pinto Jr., O., and Calheiros, R.: Lightning activity in Brazilian thunderstorms during TROCCINOX: implications for NO_x production, Atmos. Chem. Phys., 8, 921–953, https://doi.org/10.5194/acp-8-921-2008, 2008.

Iglesias-Suarez, F., Kinnison, D. E., Rap, A., Maycock, A. C., Wild, O., and Young. P. J.: Key drivers of ozone change and its radiative forcing over the 21st century, Atmos. Chem. Phys., 18, 6121–6139, https://doi.org/10.5194/acp-18-6121-2018,
25   2018.

Inness, A., Ades, M., Agustí-Panareda, A., Barré, J., Benedictow, A., Blechschmidt, A.-M., Dominguez, J. J., Engelen, R., Eskes, H., Flemming, J., Huijnen, V., Jones, L., Kipling, Z., Massart, S., Parrington, M., Peuch, V.-H., Razinger, M., Remy, S., Schulz, M., and Suttie, M.: The CAMS reanalysis of atmospheric composition, Atmos. Chem. Phys., 19, 3515–3556, https://doi.org/10.5194/acp-19-3515-2019, 2019.

Atmospheric
Chemistry
and Physics
Discussions

Jöckel, P., Tost, H., Pozzer, A., Br¨uhl, C., Buchholz, J., Ganzeveld, L., Hoor, P., Kerkweg, A., Lawrence, M. G., Sander, R., Steil, B., Stiller, G., Tanarhte, M., Taraborrelli, D., van Aardenne, J., and Lelieveld, J.: The atmospheric chemistry general circulation model ECHAM5/MESSy1: consistent simulation of ozone from the surface to the mesosphere, Atmos. Chem. Phys., 6, 5067–5104, 2006, http://www.atmos-chem-phys.net/6/5067/2006/.

5   Kerkweg, A., Buchholz, J., Ganzeveld, L., Pozzer, A., Tost, H., and Jockel, P., Technical Note: An implementation of the dry removal processes DRY DEPosition and SEDImentation in the Modular Earth Submodel System (MESSy), Atmos. Chem. Phys., 6, 4617–4632, doi:10.5194/acp-6-4617-2006, 2006.

Klein, S. A., Zhang, Y., Zelinka, M. D., Pincus, R., Boyle, J., and Gleckler, P. J.: Are climate model simulations of clouds improving? An evaluation using the ISCCP simulator, J. Geophys. Res. – Atmos., 118, 1329–1342, doi:10.1002/jgrd.50141,
10   2013.

Krause, A., Kloster, S., Wilkenskjeld, S., and Paeth H.: The sensitivity of global wildfires to simulated past, present, and future lightning frequency, J. Geophys. Res. Biogeosci., 119, 312–322, doi:10.1002/2013JG002502, 2014.

Labrador, L. J., von Kuhlmann, R., and Lawrence, M. G.: The effects of lightning-produced NO_x and its vertical distribution on atmospheric chemistry: sensitivity simulations with MATCH-MPIC, Atmos. Chem. Phys., 5, 1815–1834,
15   doi:10.5194/acp-5-1815-2005, 2005.

Lamarque, J.-F., Emmons, L. K., Hess, P. G., Kinnison, D. E., Tilmes, S., Vitt, F., Heald, C. L., Holland, E. A., Lauritzen, P. H., Neu, J., Orlando, J. J., Rasch, P. J., and Tyndall, G. K.: CAM-chem: description and evaluation of interactive atmospheric chemistry in the Community Earth System Model, Geosci. Model Dev., 5, 369–411, doi:10.5194/gmd-5-369-2012, 2012.

20   Lauer, A., Dameris, M., Richter, A., and Burrows, J. P.: Tropospheric NO_2 columns: a comparison between model and retrieved data from GOME measurements, Atmos. Chem. Phys., 2, 67–78, https://doi.org/10.5194/acp-2-67-2002, 2002.

Luhar, A. K., Galbally, I. E., Woodhouse, M. T., and Thatcher, M.: An improved parameterisation of ozone dry deposition to the ocean and its impact in a global climate-chemistry model, Atmos. Chem. Phys., 17, 3749–3767, doi:10.5194/acp-17-3749-2017, 2017.

25   Luhar, A. K., Woodhouse, M. T., and Galbally, I. E.: A revised global ozone dry deposition estimate based on a new two-layer parameterisation for air–sea exchange and the multi-year MACC composition reanalysis, Atmos. Chem. Phys., 18, 4329–4348, doi:10.5194/acp-18-4329-2018, 2018.

Luo, C., Wang, Y., and Koshak, W. J.: Development of a self-consistent lightning NO_x simulation in large-scale 3-D models, J. Geophys. Res. Atmos., 122, 3141–3154, doi:10.1002/2016JD026225, 2017.

Martin, R. V., Sauvage, B., Folkins, I., Sioris, C. E., Boone, C., Bernath, P., and Ziemke, J.: Space-based constraints on the production of nitric oxide by lightning, J. Geophys. Res., 112, D09309, doi:10.1029/2006JD007831, 2007.

Michalon, N., Nassif, A., Saouri, T., Royer, J. F., and Pontikis, C. A.: Contribution to the climatological study of lightning, Geophys. Res. Lett., 26 (20), 3097–3100, doi:10.1029/1999GL010837, 1999.

5   Miyazaki, K., Eskes, H. J., Sudo, K., and Zhang, C.: Global lightning NO_x production estimated by an assimilation of multiple satellite data sets, Atmos. Chem. Phys., 14, 3277–3305, https://doi.org/10.5194/acp-14-3277-2014, 2014.

Molinié, J., and Pontikis, C. A.: A climatological study of tropical thunderstorm clouds and lightning frequencies on the French Guyana coast, Geophysical Research Letters, 22, 1085–1088, https://doi.org/10.1029/95GL01036, 1995.

Morgenstern, O., Braesicke, P., O'Connor, F. M., Bushell, A. C., Johnson, C. E., Osprey, S. M., and Pyle, J. A.: Evaluation
10 of the new UKCA climate-composition model - Part 1: The stratosphere, Geoscientific Model Development, 2, 43–57, doi:10.5194/gmd-2-43-2009, 2009.

Murray, L. T., Jacob, D. J., Logan, J. A., Hudman, R. C., and Koshak, W. J.: Optimized regional and interannual variability of lightning in a global chemical transport model constrained by LIS/OTD satellite data, J. Geophys. Res., 117, D20307, doi:10.1029/2012JD017934, 2012.

15 Murray, L. T.: Lightning NO_x and impacts on air quality, Current Pollution Reports, 2, 115–133, doi:10.1007/s40726-016-0031-7, 2016.

Naik, V., Voulgarakis, A., Fiore, A. M., Horowitz, L. W., Lamarque, J.-F., Lin, M., Prather, M. J., Young, P. J., Bergmann, D., Cameron-Smith, P. J., Cionni, I., Collins, W. J., Dalsøren, S. B., Doherty, R., Eyring, V., Faluvegi, G., Folberth, G. A., Josse, B., Lee, Y. H., MacKenzie, I. A., Nagashima, T., van Noije, T. P. C., Plummer, D. A., Righi, M., Rumbold, S. T.,
20 Skeie, R., Shindell, D. T., Stevenson, D. S., Strode, S., Sudo, K., Szopa, S., and Zeng, G.: Preindustrial to present-day changes in tropospheric hydroxyl radical and methane lifetime from the Atmospheric Chemistry and Climate Model Intercomparison Project (ACCMIP), Atmos. Chem. Phys., 13, 5277–5298, doi:10.5194/acp-13-5277-2013, 2013.

Nault, B. A., Laughner, J. L.,Wooldridge, P. J., Crounse, J. D., Dibb, J., Diskin, G., Peischl, J., Podolske, J. R., Pollack, I. B., Ryerson, T. B., Scheuer, E., Wennberg, P. O., and Cohen, R. C.: Lightning NO_x emissions: reconciling measured and
25 modeled estimates with updated NO_x Chemistry, Geophys. Res. Lett., 44, 9479–9488, https://doi.org/10.1002/2017GL074436, 2017.

Neu, J. L., Prather, M. J., and Penner, J. E.: Global atmospheric chemistry: Integrating over fractional cloud cover, J. Geophys. Res., 112, D11306, doi:10.1029/2006JD008007, 2007.

O'Connor, F. M., Johnson, C. E., Morgenstern, O., Abraham, N. L., Braesicke, P., Dalvi, M., Folberth, G. A., Sanderson, M.
30 G., Telford, P. J., Voulgarakis, A., Young, P. J., Zeng, G., Collins, W. J., and Pyle, J. A.: Evaluation of the new UKCA

41

climate-composition model - Part 2: The Troposphere, Geoscientific Model Development, 7, 41–91, doi:10.5194/gmd-7-41-2014, 2014.

Ott, L. E., Pickering, K. E., Stenchhikov, G. L., Huntrieser, H., and Schumann, U.: Effects of lightning NO_x production during the 21 July European Lightning Nitrogen Oxides Project storm studied with a three-dimensional cloud-scale chemical transport model, J. Geophys. Res., 112, D05307, doi:10.1029/2006JD007365, 2007.

Ott, L. E., Pickering, K. E., Stenchikov, G. L., Allen, D. J., DeCaria, A. J., Ridley, B., Lin, R.-F., Lang, S., and Tao, W.-K.: Production of lightning NO_x and its vertical distribution calculated from three-dimensional cloud-scale chemical transport model simulations, J. Geophys. Res., 115, D04301, doi:10.1029/2009JD011880, 2010.

Pickering, K. E., Wang, Y., Tao, W.-K., Price, C., and Müller, J.-F.: Vertical distributions of lightning NO_x for use in regional and global chemical transport models, J. Geophys. Res., 103, 31203–31216, doi:10.1029/98JD02651, 1998.

Price, C. and Rind, D.: A simple lightning parameterization for calculating global lightning distributions, J. Geophys. Res.-Atmos., 97, 9919–9933, https://doi.org/10.1029/92JD00719, 1992.

Price, C. and Rind, D.: What determines the cloud-to-ground lightning fraction in thunderstorms? Geophys. Res. Lett., 20, 463– 466, https://doi.org/10.1029/93GL00226, 1993.

Price, C. and Rind, D.: Modeling global lightning distributions in a general circulation model, Mon. Wea. Rev., 122, 1930–1939, https://doi.org/10.1175/1520-0493(1994)122<1930:MGLDIA>2.0.CO;2, 1994.

Price, C., Penner, J., and Prather, M.: NO_x from lightning. 1. Global distribution based on lightning physics, J. Geophys. Res., 102, 5929–5941, doi:10.1029/96JD03504, 1997.

Romps, D. M., Seeley, J. T., Vollaro, D., and Molinari, J.: Projected increase in lightning strikes in the United States due to global warming, Science, 346, 851–854, https://doi.org/10.1126/science.1259100, 2014.

Rosenfeld, D. and Lensky, I. M.: Satellite-based insights into precipitation formation processes in continental and maritime convective clouds, Bull. Amer. Meteor. Soc., 79, 2457–2476, https://doi.org/10.1175/1520-0477(1998)079<2457:SBIIPF>2.0.CO;2, 1998.

Schumann, U. and Huntrieser, H.: The global lightning-induced nitrogen oxides source, Atmos. Chem. Phys., 7, 3823–3907, doi:10.5194/acp-7-3823-2007, 2007.

Telford, P. J., Abraham, N. L., Archibald, A. T., Braesicke, P., Dalvi, M., Morgenstern, O., O'Connor, F. M., Richards, N. A. D., and Pyle, J. A.: Implementation of the Fast-JX Photolysis scheme (v6.4) into the UKCA component of the MetUM chemistry-climate model (v7.3), Geosci. Model Dev., 6, 161–177, https://doi.org/10.5194/gmd-6-161-2013, 2013.

Tost, H., Jöckel, P., and Lelieveld, J.: Lightning and convection parameterisations - uncertainties in global modelling, Atmos. Chem. Phys., 7, 4553–4568, https://doi.org/10.5194/acp-7-4553-2007, 2007.

Ushio, T., Heckman, S. J., Boccippio, D. J., Christian, H. J., and Kawasaki, Z.-I.: A survey of thunderstorm flash rates compared to cloud top height using TRMM satellite data, J. Geophys. Res., 106, 24089–24095, doi:10.1029/2001JD900233, 2001.

Vonnegut, B.: Some facts and speculation concerning the origin and role of thunderstorm electricity. In: Severe Local
5   Storms. Meteorological Monographs, 5 (27), 224–241, American Meteorological Society, Boston, MA, https://doi.org/10.1007/978-1-940033-56-3_11, 1963.

Walters, D. N., Williams, K. D., Boutle, I. A., Bushell, A. C., Edwards, J. M., Field, P. R., Lock, A. P., Morcrette, C. J., Stratton, R. A., Wilkinson, J. M., Willett, M. R., Bellouin, N., Bodas-Salcedo, A., et al.: The Met Office Unified Model Global Atmosphere 4.0 and JULES Global Land 4.0 configurations, Geosci. Model Dev., 7, 361–386, doi:10.5194/gmd-7-
10   361-2014, 2014.

Williams, E. R.: Large-scale charge separation in thunderclouds, J. Geophys. Res., 90, 6013–6025, https://doi.org/10.1029/JD090iD04p06013, 1985.

Williams, E. R.: Lightning and climate: A review, Atmos. Res., 76, 272–287, https://doi.org/10.1016/j.atmosres.2004.11.014, 2005.

15   Wolfe, G. M., Nicely, J. M., Clair, J. M. S., Hanisco, T. F., Liao, J., Oman, L. D., et al.: Mapping hydroxyl variability throughout the global remote troposphere via synthesis of airborne and satellite formaldehyde observations, P. Natl. Acad. Sci. USA, 116, 11171–11180, https://doi.org/10.1073/pnas.1821661116, 2019.

Worden, H. M., Bowman, K. W., Kulawik, S. S., and A. M. Aghedo, A. M.: Sensitivity of outgoing longwave radiative flux to the global vertical distribution of ozone characterized by instantaneous radiative kernels from Aura-TES, J. Geophys.
20   Res., 116, D14115, 6013–6025, doi:10.1029/2010JD015101, 2011.

Woodhouse, M. T., Luhar, A. K., Stevens, L., Galbally, I., Thatcher, M., Uhe, P., Wolff, H., Noonan, J., and Molloy, S.: Australian reactive-gas emissions in a global chemistry-climate model and initial results, Air Quality and Climate Change, 49, 31-38, 2015.

Young, P. J., Archibald, A. T., Bowman, K. W., Lamarque, J.-F., Naik, V., Stevenson, D. S., Tilmes, S., Voulgarakis, A.,
25   Wild, O., Bergmann, D., Cameron-Smith, P., Cionni, I., Collins, W. J., Dalsøren, S. B., Doherty, R. M., Eyring, V., Faluvegi, G., Horowitz, L. W., Josse, B., Lee, Y. H., MacKenzie, I. A., Nagashima, T., Plummer, D. A., Righi, M., Rumbold, S. T., Skeie, R. B., Shindell, D. T., Strode, S. A., Sudo, K., Szopa, S., and Zeng, G.: Pre-industrial to end 21st century projections of tropospheric ozone from the Atmospheric Chemistry and Climate Model Intercomparison Project (ACCMIP), Atmos. Chem. Phys., 13, 2063–2090, doi:10.5194/acp-13-2063-2013, 2013.

30   Zhu, Q., Laughner, J. L., and Cohen, R. C.: Lightning NO_2 simulation over the contiguous US and its effects on satellite NO_2 retrievals, Atmospheric Chemistry and Physics, 19, 13067–13078, https://doi.org/10.5194/acp-19-13067-2019, 2019.